Research Square

Preprints are preliminary reports that have not undergone peer review.
They should not be considered conclusive, used to inform clinical practice,
or referenced by the media as validated information.

The effect of lanthanum and iodine co-doping on the photosensitive properties of chemically-bath-deposited PbS films

Larisa Maskaeva
Ural Federal University Named After the First President of Russia B.N. Yeltsin
Timofey Bokov
Ural Federal University Named After the First President of Russia B.N. Yeltsin
Elena Mostovshchikova
mostovsikova@imp.uran.ru

M.N. Mikheev Institute of Metal Physics of Ural Branch of Russian Academy of Sciences
Vladimir Voronin
M.N. Mikheev Institute of Metal Physics of Ural Branch of Russian Academy of Sciences
Oleg Eltsov
Ural Federal University Named After the First President of Russia B.N. Yeltsin
Andrey Pozdin
Ural Federal University Named After the First President of Russia B.N. Yeltsin
Irina Miroshnikova
National Research University "Moscow Energy Institute"
Ivan Lobov
M.N. Mikheev Institute of Metal Physics of Ural Branch of Russian Academy of Sciences
Tamara Kuznetsova
Institute of High Temperature Electrochemistry of Ural Branch of Russian Academy of Sciences

Research Article

Keywords: lead sulfide, chemical bath deposition, iodine and lanthanum co-doling, synergetic effect, photoresponse

Posted Date: September 2nd, 2026

DOI: https://doi.org/10.21203/rs.3.rs-10428826/v1

License: This work is licensed under a Creative Commons Attribution 4.0 International License.
Read Full License

Additional Declarations: No competing interests reported.

The effect of lanthanum and iodine co-doping on the photosensitive properties of chemically-bath-deposited PbS films

Maskaeva L.N.[1,2], Bokov T.S.[1], Mostovshchikova E.V.[3,*], Voronin V.I.[3], Eltsov O.S.[1], Pozdin A.V.[1], Miroshnikova I.N.[4], Lobov I.D. [3], Kuznetsova T. A.[5]

[1]Ural Federal University Named After the First President of Russia B.N. Yeltsin, Ekaterinburg 620062, Russian Federation

[2]Ural Institute of State Fire Service of EMERCOM of Russia, Ekaterinburg 620062, Russian Federation

[3]M.N. Mikheev Institute of Metal Physics of Ural Branch of Russian Academy of Sciences, Ekaterinburg 620077, Russian Federation

[4]National Research University "Moscow Energy Institute", Moscow, 111250, Russian Federation

[5] Institute of High Temperature Electrochemistry, of Ural Branch of Russian Academy of Sciences, Ekaterinburg 620066, Russian Federation

*Corresponding author. E-mail: mostovsikova@imp.uran.ru

Abstract. Films of PbS, PbS(I), PbS(La), and PbS(La, I) with were obtained by chemical bath deposition. Their composition, morphology, crystal structure, optical and photosensitive properties were studied. A synergistic effect of increasing the photosensitivity of PbS films with combined doping was revealed, effectively increasing the photosensitivity, especially at low concentrations (1 mM) of $LaCl_3$ in the presence of ammonium iodide NH_4I, caused by the formation of a synergistic pair of the optically active phase of diiodine pentoxide I_2O_5 and lanthanum oxide La_2O_3 on the crystallite surface. Comparing data on dependence of band gap E_g and photosensitive properties of PbS(La, I) films indicates that the main factor influencing the achievement of a high photoresponse in the form of high voltage sensitivity is an increase in the proportion of nanoparticles in the composition of the formed polycrystalline films.

Keywords: lead sulfide; chemical bath deposition; iodine and lanthanum co-doling; synergetic effect; photoresponse

Relevance Summary

Production of PbS films by chemical bath deposition with co-introduction of a donor (La^{3+}) and acceptor (I^-) additive leads to significant increase in photoresponse.

It is explained by a synergistic effect of La_2O_3 and I_2O_5 impurity phases formed on surface of crystallites of PbS films.

Co-doping with (La3+) and (I-) salts to produce highly photosensitive PbS films has used for the first time.

Proposed one-pot method to enhance photosensitivity of PbS films is important for optoelectronics.

1. Introduction

One of the most promising and multifunctional semiconductor, which is of great interest for fundamental research, is lead sulfide PbS being a representative of the A^{IV}-B^{VI} family of semiconductor compounds. Lead sulfide has a high permittivity (ε_{PbS} = 15-20), absorption coefficient in the visible and near infrared spectral range ($\sim 10^5$ cm^{-1}), mobility ($\sim$29.3 $cm^2V^{-1}s^{-1}$) and carrier concentration ($\sim 10^{-18}$ cm^{-3}) [1], as well as the ability to significantly expand the band gap from 0.3 to 5.2 eV during the transition to the nanostate [2, 3]. The main focus of researchers is on studying the properties and modification methods of polycrystalline lead sulfide films. The choice of thin-film lead sulfide PbS as an object of study is caused by its wide range of practical applications associated with high level of photosensitivity in the visible and near-IR spectral range (0.4–3.0 μm) [4-10], long-term photostability and radiation resistance [11], high efficiency of solar energy conversion [12], prospects for use in night vision devices [13], medical imaging [14], fire alarm sensors for early detection of fire sources [15], as relatively cheap thermoelectric materials [16], chemical sensors for monitoring toxic substances in the air [17-19] and heavy metals in the aquatic environment [20], as well as remote monitoring of atmospheric pollution [21].

Modifying semiconductor materials by changing their dimensionality or doping has not only practical but also fundamental significance. To broad the range of radiation received by PbS-based detectors the electronic and optical properties are modified by doping them with donors or acceptors [22], which are centers of radiative (non-radiative) recombination of nonequilibrium charge carriers. Systematic change of the properties of PbS films synthesized by chemical bath deposition (CBD) or spray pyrolysis (simple and inexpensive methods of synthesis) were carried out by introducing into the reaction mixture a donor impurity in the form of salts of alkali (Li^+, Na^+, K^+) [23, 24], alkaline earth (Mg^{2+} [25-27], Ca^{2+}[28, 29], Sr^{2+}[30, 31], Ba^{2+} [32]), as well as transition (Cr^{3+} [33], Mn^{2+} [34], Fe^{2+} [35], Co^{2+} [36-38], Ni^{2+} [39]) metals. It has been shown that lead sulfide films with such doping retain the *n*-type conductivity, just like undoped metal sulfide, due to the excess of lead atoms [40]. Our studies have shown that chemically deposited *n*-type lead sulfide films have no significant photosensitivity. On the other hand, cationic doping of polycrystalline PbS films with an anionic

component (iodine I^-) provides them with a relatively high voltage sensitivity to IR radiation due to the inversion of conduction bands (n → p) at anomalously small values of the time constant [41]. The simultaneous introduction of anionic and cationic additives into the CBD reaction mixture (for example, a combination of salts containing I^- and Ni^{2+}) is accompanied by an increase in voltage sensitivity by approximately 1.7 times compared to doping with iodine alone [39].

Among the approaches for modifying narrow-band lead sulfide the introduction of rare earth metals [42, 43] should be noticed, which is widely used in innovative scientific and technical fields such as the production of catalysts, magnetic, luminescent, optical and photosensitive materials, as well as for biomedical applications [44-49]. Rare earth metal impurities, when introduced into PbS crystal lattice or replacing lead ions, result in changes in the band structure and the formation of "deep" levels in the band gap, and, as a consequence, to a change in the functional properties. In particular, cerium Ce impurity ions in lead sulfide improve its dielectric and electrical properties [50], gadolinium Gd increases transparency and optimizes magnetic properties [51] and also provides high transmittance and chemical stability [52], europium Eu [53] and neodymium Nd [54] increase photosensitivity and provide nonlinear optical properties which make it possible to recommend the discussed metal sulfide for use in optoelectronics [55]. PbS films doped with samarium Sm are a potential candidate for use in photosensors [56], praseodymium Pr is recommended for use in optoelectronic devices [57, 58], and terbium Tb ensures the production of the most effective luminescent materials [59]. An analysis of the scientific literature from the past few years shows, that La-doped lead sulfide films may be an interesting subject for research. In particular, doping with lanthanum La will lead to more efficient electron-hole separation, enhancing its effect on functional properties, which will enable its use in photonics, photovoltaics, photoconductivity, fast optical switching, and information processing [60].

Studies of co-doping of a narrow-gap semiconductor (in our case, PbS) containing a large number of intrinsic defects with a combined donor-acceptor additive [39] indicate the potential of the proposed one-pot approach to the synthesis of PbS semiconductor films suitable for highly functional IR photodetector devices. By now, co-doping of PbS films with iodine and lanthanum was not considered in literature, therefore, in this paper we present experimental results on the structural, optical, and photosensitive properties of lead sulfide films doped with a combination of lanthanum and iodine ions during chemical bath deposition from aqueous solutions.

2. Experimental

Thin-film layers of lead sulfide were obtained by CBD from aqueous solutions containing 0.04 M lead acetate $Pb(CH_3COO)_2$, 0.3 M sodium citrate $Na_3C_6H_5O_7$, 4.0 M ammonium

hydroxide NH_4OH and 0.58 M thiourea $(NH_2)_2CS$. Doping of PbS films with lanthanum La^{3+} during CBD was carried out by additionally introducing from 0.01 to 10 mM lanthanum chloride $LaCl_3$ into the reactor; doping with iodine was carried out by adding from 0.05 to 0.25 M ammonium iodide NH_4I.

In simplified terms, the CBD process of lead sulfide PbS doped with lanthanum and iodine is a set of complex intermolecular interactions in the volume of the system between free ions of lead Pb^{2+} and lanthanum La^{3+} with thiourea in the presence of ammonium iodide in an alkaline medium [61], and can be written as the following reaction

$$La^{3+} + Pb^{2+} + NH_4I + N_2H_4CS + 4OH^- = PbS(La, I)\downarrow + CN_2^{2-} + NH_4^+ + 4H_2O. \quad (1)$$

Lead sulfide films deposited from the reaction mixture in the presence of a combination of ammonium iodide with lanthanum(III) chloride, only lanthanum chloride, only ammonium iodide or without doping are designated as PbS(La, I), PbS(La), PbS(I), and PbS. The films were deposited on pre-degreased glass slide substrates (72.2% SiO_2, 14.3% Na_2O; 1.2% K_2O, 6.4% CaO, 4.3% MgO, 1.2% Al_2O_3, 0.03% Fe_2O_3, 0.3% SO_3) for 90 min at 353 K in a TS-TB-10 liquid thermostat, which ensured temperature maintenance accuracy of ±0.1 K.

The thickness of the obtained films was determined using an interference microscope (Linnik microinterferometer) MII-4M with a measurement error of 10%.

A Tescan Vega 4 LMS scanning electron microscope (SEM) with an Oxford Xplore EDS – AZtecOne energy-dispersive X-ray spectroscopy (EDS) module was used to study the morphology and elemental composition of the films. Particle size was calculated using Measurer software, and further data processing was performed using the Grapher and Origin software packages.

X-ray structural studies of the films were carried out by X-ray diffraction (XRD) on a Bruker-8 diffractometer with a CuK_α copper anode in the angle range of $2\theta = 20–80°$ with a step of 0.01° and a scanning time of 1.5 s per point. The experimental XRD patterns were described using the Rietveld full-profile analysis [62] in the GSAS-2 program [63]. The scale factor, spectral zero shift, deviation from the scattering plane, and Debye-Waller thermal factor were preliminarily refined in the calculations, and the Chebyshev polynomial was used to describe the XRD pattern background [64].

To separate the contributions of grain size and deformation in the studied films to the width of XRD reflections the *conventional* Williamson–Hall plot was used [65]:

$$\beta \times \cos\theta = 0.9\lambda/D + 4\varepsilon \times \sin\theta. \quad (2)$$

Here D is the average size of the coherent scattering regions (CSR) β is the half-width of the XRD reflection in radians, λ is the wavelength of the X-ray radiation used, $\varepsilon = \Delta d/d$ is the microdeformation, d is the interplanar distance.

Fourier transform infrared (FTIR) spectra of the synthesized films were recorded in a transmission mode by a Fourier spectrometer Bruker Alpha, the ATR attachment (ZnSe), within the range of 500−2000 cm^{-1} with the resolution of 4 cm^{-1}. FTIR data were obtained in Laboratory of Complex Research and Expert Evaluation of Organic Materials, Center for Collective Use of unique equipment of the Ural Federal University.

The absorption spectra αI in the 0.25–0.9 eV range (2000–7240 cm^{-1}, resolution 4 cm^{-1}) were calculated from the light transmission spectra tI measured at room temperature using a Frontier IR Single-Range Spectrometer (PerkinElmer, UK) by using the formula:

$$\alpha(E) = \frac{1}{d_f} \ln\left(\frac{1}{t(E)}\right), \quad (3)$$

where d_f is the film thickness, tI = I/I_0 is the film transmittance, I, I_0 are the intensity of light transmitted through the film and through the substrate, respectively; the reflection coefficient was not taken into account.

To study the photoelectric properties of the films, 5×5 mm sensor elements with electrochemically deposited ohmic nickel contacts were fabricated. The photoelectric characteristics (dark resistance R_d, voltage sensitivity U_s) of the films were measured using a K54.410 setup with a black body radiation source with a temperature of 673K at a radiation modulation frequency of 1000 Hz, a bias voltage of 20 V, and an irradiance of 1×10^{-4} W/cm^2.

The conductivity type of the deposited films was determined by the sign of the thermoelectric power when creating a temperature gradient in the area of the probe contacts.

3. Results and discussion

3.1. Thermodynamics and kinetics of the formation of PbS, La_2S_3, $Pb(OH)_2$, $La(OH)_3$ in the system "$Pb(CH_3COO)_2 – LaCl_3 – Na_3C_6H_5O_7 – NH_4OH – N_2H_4CS$"

It is known [66] that the kinetic-thermodynamic approach makes it possible not only to confirm the fundamental possibility of implementing the process, but also to purposefully control and predict its results by elucidating the mechanism. Therefore, for a comprehensive understanding of the chemical precipitation of lead sulfide, thermodynamic modeling of the boundary conditions for the formation of poorly soluble compounds in the form of PbS and La_2S_3, as well as impurity phases of lead and lanthanum hydroxides $Pb(OH)_2$ and $La(OH)_3$ in the system "$Pb(CH_3COO)_2$ – $LaCl_3$ – $Na_3C_6H_5O_7$ (Na_3Cit) – NH_4OH – NH_4I – N_2H_4CS(TM)" was initially carried out using the method proposed in [66], which makes it possible to determine the composition of the reaction mixture.

In simplified terms, the process of chemical co-deposition of lead sulfides and lanthanum PbS and La_2S_3, which is a set of intermolecular interactions in the volume of the system between

complexed lead PbL_1^{2+} and lanthanum LaL_2^{3+} ions with thiourea in an alkaline medium, can be written as the reaction [66, 67]

$$PbL_1^{2+} + LaL_2^{3+} + N_2H_4CS + 4OH^- = PbS(La)\downarrow + L_1 + L_2 + CN_2^{2-} + 4H_2O, \quad (4)$$

where L_1 and L_2 are ligands for lead and lanthanum ions, respectively.

As a first approximation, the following equality serves as a criterion for the formation of metal sulfide in dilute solutions:

$$IP_{MeS} = SP_{MeS}, \quad (5)$$

where IP_{MeS} is the ionic product of sulfide PbS (La_2S_3), that is, the product of the concentrations of uncomplexed forms of metals Pb^{2+} (La^{3+}) and the sulfide ion S^{2-}; SP_{MeS} is the solubility product of the solid phase of lead sulfide PbS or lanthanum sulfide La_2S_3.

To compensate for the excess surface energy of nucleation and the stable formation of a solid phase of metal sulfides, it is necessary to exceed the ionic product IP of the compound over its solubility product SP, i.e. to create supersaturation Δ

$$\Delta > IP_{(PbS,La_2S_3)}/SP_{(PbS,La_2S_3)} \quad (6)$$

The magnitude of supersaturation Δ arising in the reaction system was determined by the amount of free metal ions [Me^{n+}] (Pb^{2+} or La^{3+}), the fractional concentration of which was estimated by the expression

$$\alpha_{Me^{n+}} = \frac{[Me^{n+}]}{C_{Me^{n+}}} = \frac{1}{1+\frac{[L_1]}{k_1}+\frac{[L_{1,2}]^2}{k_{1,2}}+\cdots\frac{[L_{1,2\ldots n}]^n}{k_{1,2\ldots n}}} \quad (7)$$

Here $C_{Me^{n+}}$ is the total concentration of metal ions in solution; [L_1], [$L_{1,2}$], [$L_{1,2\ldots n}$] are concentrations of ligands; k_1, $k_{1,2}$, $k_{1,2\ldots n}$ are instability constants of metal complexes. The analysis of ionic equilibria was carried out taking into account all known complex forms of lead Pb^{2+} and lanthanum La^{3+} ions formed in the reaction mixture under discussion [68, 69]. The contribution to the total concentration of lead and lanthanum ions present in the solution in the form of complexes was calculated similarly to (7), substituting the concentration of the corresponding complex into the numerator of the expression instead of the concentration of the free lead ion. The results of calculating complex compounds of Pb^{2+} and La^{3+} ions using the approach proposed by Butler N. [70] showed that the decisive contribution to the total concentration of lead ions is made by the hydroxycitrate complex $Pb(OH)Cit^{2-}$, the share of which at pH = 9-12 is close to unity; with an increase in pH > 12 its share decreases and at pH = 13 the lead hydroxocomplex $Pb(OH)_4^{2-}$ begins to predominate. Calculations show that at pH >10, the formation of fairly strong lanthanum citrate complexes is possible, especially $La(Cit)_2^{3-}$, the fraction of which is close to unity. As shown in [41], lead ions form weak complexes with iodide ions, and complexes of lanthanum ions with iodine ions could not be found.

Taking into account the size of the critical nuclei depending on the nature of the ligands for Pb^{2+} (La^{3+}) ions, the minimum required concentrations of salts of these metals were estimated to ensure the formation of solid phases of PbS and La_2S_3 using the expression [66]

$$pC_{\text{i}} = pSP_{\text{MeS}} - p\alpha_{\text{Me}^{2+}} - (pk_{\text{H}_2\text{S}}^{1,2} + \frac{1}{2}pK_{\text{c}} - 2pH + \frac{1}{2}p[\text{N}_2\text{H}_4\text{CS}]_{\text{i}} - \frac{1}{2}p\frac{\beta_{\text{c}}}{\beta_{\text{S}}}) - \frac{0.86\,\sigma\,V_{\text{M}}}{R\,T\,r_{\text{cr}}}, \quad (8)$$

where p is an exponent (negative decimal logarithm); C_{i} is an initial (minimum) concentration of lead (lanthanum) salt required to form a solid phase PbS (La_2S_3); SP_{MeS} – solubility product of metal sulfide, $pSP_{\text{PbS}} = 27.1$ and $pSP_{\text{La}_2\text{S}_3} = 12.7$ [71]; $k_{\text{H}_2\text{S}}^{1,2}$ is an ionization constant of hydrogen sulfide, $pk_{\text{H}_2\text{S}}^{1,2} = 19.88$ [69]; values β_{c} and β_{S} determined as $\beta_{\text{S}} = [\text{H}_3\text{O}^+]^2 + k_{\text{HS}^-}[\text{H}_3\text{O}^+] + k_{\text{H}_2\text{S}}$; $\beta_{\text{c}} = [\text{H}_3\text{O}^+]^2 + k_{\text{HCN}_2^-}[\text{H}_3\text{O}^+] + k_{\text{H}_2\text{CN}_2}$; K_{c} is a constant of hydrolytic decomposition of thiourea $pK_{\text{c}} = 22.48$ [66]; $[N_2H_4CS]_{\text{i}} = 0.58$ M is an initial concentration of thiourea; $\sigma = 1.0$ J/m^2 is a specific surface energy of metal sulfide (surface tension) [66]; V_{M} is a molar volume of synthesized phase, $V_{\text{M(PbS)}} = 3.32\times10^{-5}$ m^3/mol, $V_{\text{M}(\text{La}_2\text{S}_3)} = 9.14\times10^{-5}$ m^3/mol; $r_{\text{cr}} = 3.5\times10^{-9}$ m is a critical nucleus radius [66]; $R = 8.31$ J/(mol K) is the universal gas constant; $T = 298$ K is a temperature.

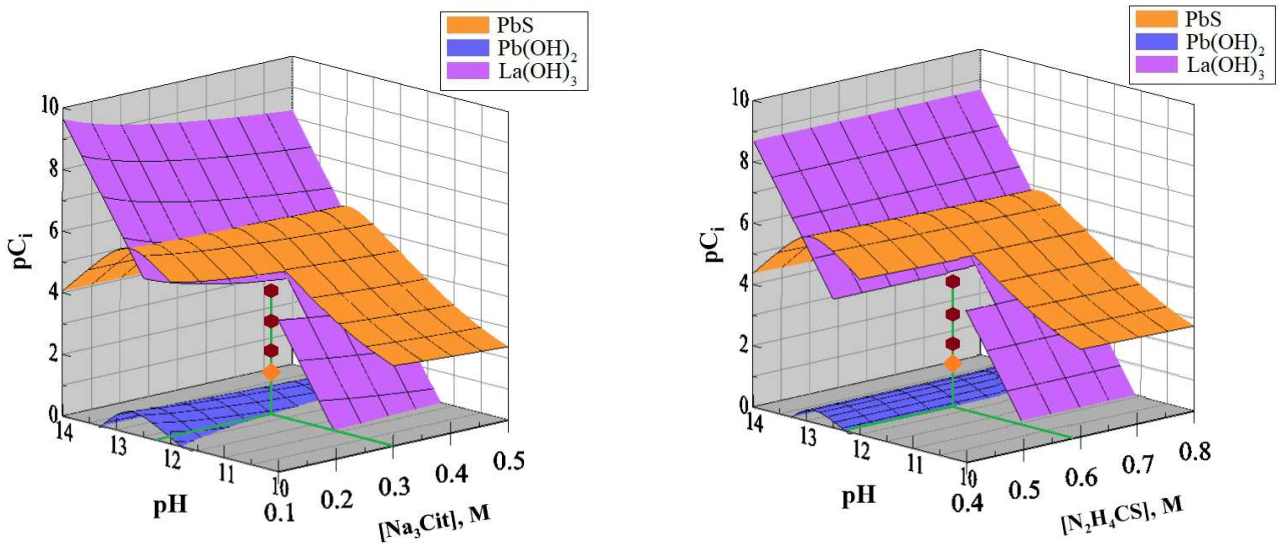
During chemical bath deposition, in addition to the formation of lead and lanthanum sulfides, side reactions occur, producing lead hydroxides $Pb(OH)_2$, lanthanum hydroxides $La(OH)_3$, and lead cyanamide $PbCN_2$. The inclusion of these impurity phases in the lead and lanthanum sulfides can affect the electrical and functional properties of the films. The following expressions were used to predict their formation:

$$pC_i = pSP_{\text{Me(OH)}_\text{n}} - p\alpha_{\text{Me}^{\text{n}+}} - npK_{\text{W}} + n\text{pH}\ , \quad (9)$$

where $SP_{\text{Me(OH)}_n}$ is the solubility product of the metal hydroxide, $pSP_{\text{Pb(OH)}_2} = 14.84$ and $pSP_{\text{La(OH)}_3} = 18.7$ [71]; K_{W} is the ionic product of water, n is the charge of the metal ions.

The results of calculations of the boundary conditions for the formation of PbS, as well as the impurity phases $Pb(OH)_2$ and $La(OH)_3$ in the form of three-dimensional graphical dependencies in the coordinates "pCi – pH of the solution – [Na3Cit]" and "pCi – pH of the solution – N_2H_4CS]" are shown in Fig. 1. Below the concentration surfaces corresponding to the solid phases PbS (orange), Pb(OH)2 (blue), La(OH)3 (lilac), their formation is possible. As for the solid phase La_2S_3, its formation is unlikely, since sufficiently high concentration of lanthanum salt (up to 10^{-3} M) is required, the creation of which is impossible in the used reaction mixture. In the alkaline region (pH = 13-14), only lanthanum hydroxide can form between the $La(OH)_3$ (pink) and PbS (orange) concentration planes. At the intersection of these concentration planes and below the $Pb(OH)_2$ plane, the simultaneous chemical deposition of lead sulfide and lanthanum hydroxide can be expected. Below the concentration plane responsible for the formation of $Pb(OH)_2$ (blue), at pH = 12.0-13.5, the formation of lead and lanthanum

hydroxides, as well as lead sulfide, is expected. Thus, the calculations of the boundary conditions for the deposition of the poorly soluble compounds under discussion let conclude that the formation of solid solutions based on lead and lanthanum sulfides is impossible, but there is a possibility of lanthanum entering lead sulfide in the form of its hydroxide at the intersection or below the concentration planes of PbS and $La(OH)_3$.

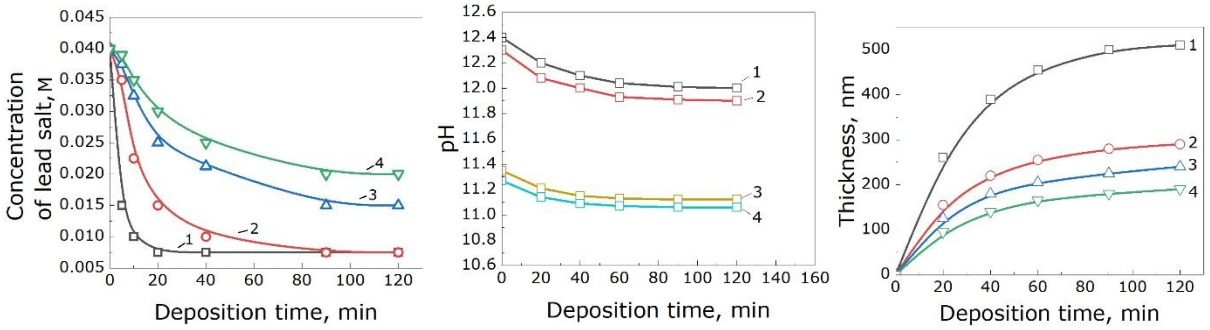


a b

Fig. 1 Boundary conditions for the formation of solid phases of PbS, $Pb(OH)_2$, $La(OH)_3$ on pH in the system "$Pb(CH_3COO)_2$ – $LaCl_3$ – Na_3Cit – NH_4OH – N_2H_4CS" with a change in the concentration of sodium citrate (a) and thiourea (b). Boundary conditions were calculated at $[N_2H_4CS]$ = 0.58 M (a), $[Na_3Cit]$ = 0.3 M (b), $[NH_4OH]$ = 4 M (a, b) and at temperature of 298 K. The optimal concentrations of salts $Pb(CH_3COO)_2$ and $LaCl_3$ are designated as orange rhomb and wine-red hexahedrons, respectively.

For the kinetic studies, a reaction mixture containing 0.04 M $Pb(CH_3COO)_2$, 4 M NH_4OH, 0.58 M N_2H_4CS and dopants of 1 mM $LaCl_3$, 0.17 M NH_4I, or a combination thereof, was selected. The kinetic curves (Fig. 2a) show that the formation of the solid phase of lead sulfide in the absence of a dopant is characterized by a fairly high rate (curve 1): 10 minutes after the start of the CBD process, the lead acetate concentration decreases from 0.04 to 0.01 M, and equilibrium in the system is established by the 40th minute. The introduction of 1 mM $LaCl_3$ into the reaction mixture shifts the equilibrium to the 90th minute (curve 2), by which time approximately 94% of the lead acetate has already been consumed. With the addition of 0.17 M NH_4I (curve 3), the rate of lead acetate conversion to sulfide is reduced, and the kinetic curve becomes more gradual. By the time equilibrium is reached (90 minutes from the start of the CBD process), 85% of the lead salt has been consumed. The most pronounced inhibitory effect is observed with the simultaneous presence of 1 mM LaCl3 and 0.17 M NH_4I in the reactor (curve

4). In this case, the process is significantly slowed: even by the 120th minute, the lead salt concentration remains at 0.02 M, i.e., the conversion of lead salt to sulfide has only been 50%.



a b c

Fig. 2 Kinetic curves of the conversion of lead salt into sulfide (a), change in pH in the reaction mixture (b), and change in film thickness (c) for the films PbS (curve 1), PbS(La) ([$LaCl_3$]= 1 mM, curve 2), PbS(I) ([NH_4I]=0.17 M, curve 3), and PbS(La,I) ([$LaCl_3$]=1 mM and NH_4I=0.17 M, curve4). Temperature of CBD was 353 K

During the CBD process pH values of the reaction mixture decreases (Fig.2b) from 12.4 and 12.3 for PbS (curve 1) and PbS(La) (curve 2) to ~12.0 and 11.9, respectively. These pH values are in the favorable range (11.8–12.2) for the hydrolytic decomposition of thiourea being a key step in the synthesis [66], i.e. thiourea supplies a sufficient amount of S^{2-} ions to the reaction mixture. The chemical deposition of PbS(I) and PbS(La,I) films from reaction mixtures in the presence of 0.17 M NH_4I (curve 3) or combination 0.17 M NH_4I and 1 mM $LaCl_3$ (curve 4) is carried out at initial pH values of ~11.32 and 11.28, respectively, which decrease to ~11.1 and 11.0 upon completion of the process. Such a decrease in pH slows down the hydrolytic decomposition of thiourea giving sulfur ions S^{2-} probably due to the inhibitory effect of ammonium iodide.

As a result of change in kinetic and pH during CBD of considered PbS, PbS(La), PbS(I), and PbS(La,I) films the thickness d_f of the obtained films differs (Fig. 2c): d_f of PbS(La) film is approximately 1.3 times thinner than that of the PbS film. This is probably due to the adsorption of lanthanum La^{3+} and chlorine Cl^- ions on the surface of growing PbS crystallites and colloidal $Pb(OH)_2$ particles, as well as the formation of poorly soluble lead compounds PbOHCl (K_{sp} = 2×10^{-14}) and $PbCl_2$ (K_{sp} = 1.6×10^{-5}) [69], which disrupt the ordering of the crystal lattice. By blocking active centers on the substrate, the number of available sites for nucleation decreases, which leads to a slowdown in the growth of lead sulfide film crystallites. In the case of PbS(I) and PbS(La,I) films the combination of the effects of decreasing the concentration of sulfur ions with a simultaneous decrease in the concentration of free Pb^{2+} ions due to the formation of poorly soluble lead compounds, in addition to the previously mentioned PbOHCl, $PbCl_2$, also

includes PbOHI (K_{sp} = 8.7×10^{-9}) [71] and PbI_2 (K_{sp} = 8.7×10^{-9} [71], 1.1×10^{-9} [69]), leads to a decrease in the ionic product IP = [Pb^{2+}]*[S^{2-}] and as a result significant decrease in thickness of the films.

Figure 3 shows dependence of the thickness d_f of PbS(La) and PbS(I) films on a concentration of ammonium iodide NH_4I or lanthanum chloride $LaCl_3$ in the reaction bath and that of PbS(La, I) films deposited with presence of fixed content of [$LaCl_3$] = 1 mM deposited during 90 min at T=353 K. An increase in the concentration of NH_4I or $LaCl_3$ in the reaction mixture results in a decrease in the thickness of PbS(I) and PbS(La) films by approximately 2.3 and 2.8 times compared to the undoped PbS film. In the case of PbS(I) films, this effect is explained by a decrease in the concentration of sulfur ions S^{2-} and lead Pb^{2+} with a decrease in the pH of the solution in the presence of ammonium iodide, which inhibits the rate of hydrolytic decomposition of thiourea N_2H_4CS and the formation of poorly soluble lead compounds PbOHI and PbI_2 [41]. In the case of competing reactions in a thiourea solution with additives of lead and rare earth metal salts, the S^{2-} ion will act as a site of ion-coordination interaction with the cations of both lead ions Pb^{2+} and the doping metal La^{3+} [72]. Considering the closer chemical affinity of sulfur S^{2-} to lead Pb^{2+} than to lanthanum La^{3+}, it is with lead that the interaction with the formation of thiourea complex compounds in solution should occur first. Pb^{2+} ions form octahedral complexes, interacting with 4-6 thiourea molecules, whereas La^{3+} ion can form more complex structures, coordinating with 6-8 thiourea molecules creating unfavorable conditions for the formation of a solid lead sulfide phase on the substrate. As a result, a twofold decrease in the thickness of PbS(La) films is observed. For PbS(La, I) films the combined addition of a rare earth metal salt (1 mM of $LaCl_3$) and ammonium iodide with varying concentrations in the solution effects PbS(La, I) film thickness less. For these films, the dependence of the deposited layer thickness on the NH_4I concentration is flatter, with the thickness decreasing by only 1.5 times compared to the PbS(La) film.

3.3. Morphology and elemental analysis

SEM images with histograms of the crystallite size distribution in Figure 4 show an evolution of the morphology (the size, shape and orientation of the grains) of PbS(La) films deposited from the reaction bath containing $LaCl_3$ with varying concentration from 0.01 to 5.0 mM. For comparison, a SEM image of an undoped PbS film is shown in Figure 4a. It is seen that PbS film consists of crystallites with clearly defined faceting, the main proportion (~60-65%) of which is in the size range of 400-1000 nm, including larger crystallites of 1.4-1.8 μm, which indicates their intensive growth in the absence of doping additives. The introduction of $LaCl_3$ into the reaction bath does not destroy the crystallite faceting. At low concentrations of the $LaCl_3$

doping salt a portion of crystallites with the size of 400-1000 nm increases to ~81% and the rate of large crystallites (1.1-1.2 μm) decreases (Fig. 4 b, c). It indicates partial suppression of the processes of the crystallites coarsening.

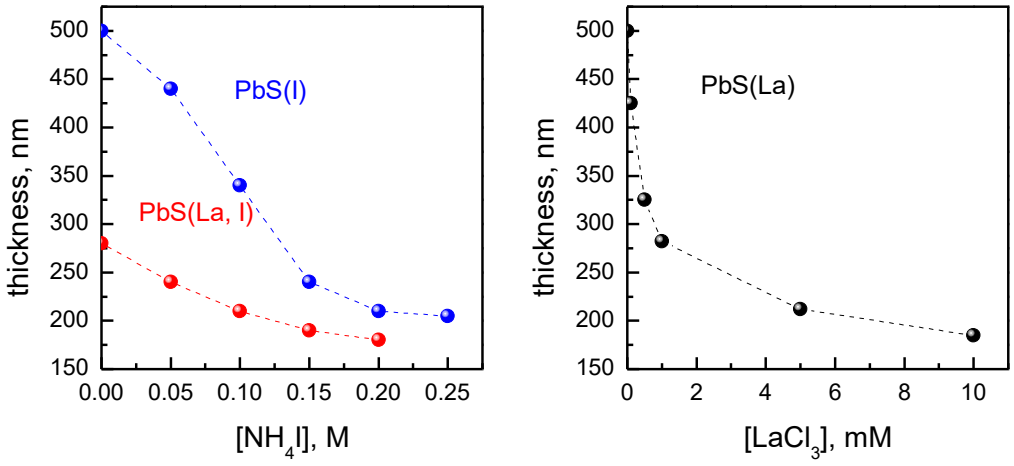


Fig. 3 Dependence of the thickness of PbS(I), PbS(La), and PbS(La, I) films on the concentration of ammonium iodide NH_4I or lanthanum chloride $LaCl_3$. For PbS(La, I) films dependence was obtained at fixed concentration 1 mM of $LaCl_3$

The observed refinement of the lead sulfide film microstructure can be explained by the theory of heterogeneous nucleation. Trivalent La^{3+} ions, which possess high surface activity and selectively adsorb on active substrate sites and colloidal $Pb(OH)_2$ particles, create steric and electrostatic barriers to the diffusion of Pb^{2+} and S^{2-} ions to the substrate surface. As a result, the growth rate of individual grains is suppressed, while the rate of formation of new fluctuation crystallization centers increases. This controlled regime results in the formation of denser PbS(La) films from finely dispersed grains.

With a further increase in the $LaCl_3$ concentration to 0.5-1.0 mM, a more pronounced refinement of the crystallites of PbS(La) films is observed (Fig. 4 d, e). The majority of crystallites (up to 70-78 %) are in the range of 200-600 nm, and the size distribution becomes narrower with a monomodal character. It should be noted that the shape of the grains is preserved. The concentration 5 mM of $LaCl_3$ leads to an expansion of the crystallite size range (Fig. 4f) and the appearance of an additional contribution of larger crystallites (up to 1.2-1.4 μm), which may be due to the competition between the nucleation and growth processes of PbS(La) film under conditions of an increased La^{3+} content in the solution. Thus, the introduction of $LaCl_3$ influences the formation of PbS(La) film, leading to a change in the crystallite sizes of the lead sulfide film while maintaining their faceting.

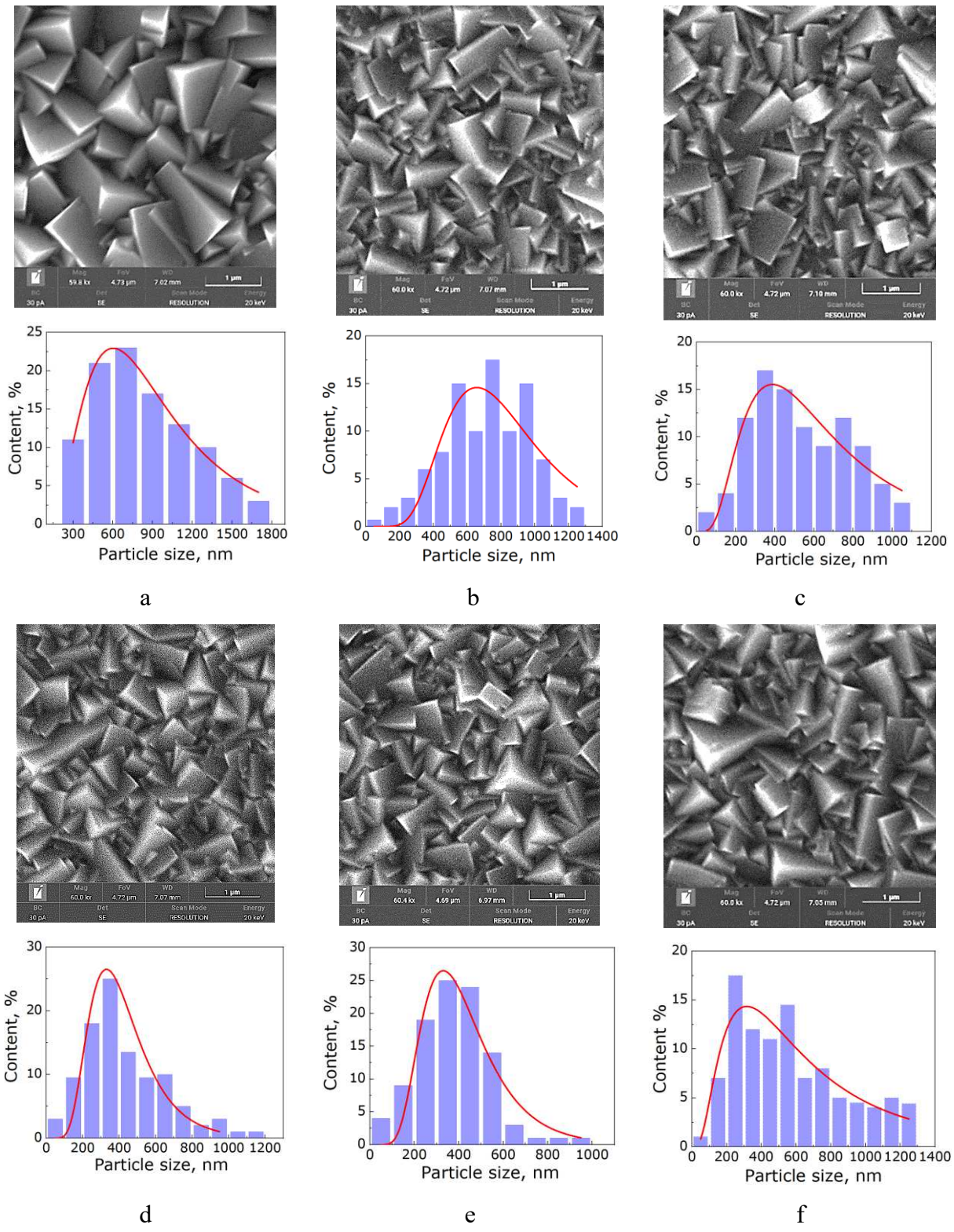


Fig. 4 SEM images and histograms of crystallite size distribution in PbS (a) and PbS(La) films with different content of $LaCl_3$ in the reaction mixture: 0.01 (b), 0.1 (c), 0.5 (d), 1 (e), and 5.0 mM (f)

Analysis of the SEM data revealed that the introduction of $LaCl_3$ is an effective tool for controlling the size and orientation of the crystallites that form lead sulfide films. To

quantitatively analyze the microstructural changes in PbS films upon the introduction of the dopant, statistical processing of the experimental grain size distribution histograms reported in Fig. 4 was performed, and their approximation was performed using the theoretical lognormal distribution function (Fig. 5). In Figs. 5a, c median (divides the grain size distribution in half), mode (most probable grain size), arithmetic mean parameter μ (mathematical expectation of the logarithms of grain sizes), and FWHM (full width of the curve at a level equal to half its maximum height) are shown. As can be seen from Fig. 5a, the particle size distribution parameters reach a minimum at 1 mM $LaCl_3$ in the reaction mixture. At this point, the system exhibits nontrivial behavior, likely due to the formation of a dominant fine grain fraction within the PbS(La) films. Figure 5b shows content of nanoparticles in PbS(La) films depending on the concentration of $LaCl_3$ in the reaction bath. It is seen, that maximal portion of nanoparticles is found in the film deposited from the solution containing 1 mM of lanthanum chloride. Therefore there is a correlation between decrease in particle size of crystallites forming PbS(La) films and increase in nanoparticles content at adding $LaCl_3$ into reaction mixture. This suggests that the dopant ions, which influence nucleation, create optimal conditions for obtaining the most monodisperse PbS film by stabilizing the intermediate phase and determining the desired grain growth dynamics. According to experimental data, a dopant concentration of 1 mM lanthanum chloride provides maximum control over grain size and the degree of monodispersity. As photosensitive properties of PbS films depends on crystallite surface size, Figs 5 a and b let conclude that concentration 1 mM $LaCl_3$ is optimal for used reaction mixture "$Pb(CH_3COO)_2$ – $LaCl_3$ – $Na_3C_6H_5O_7$ – NH_4OH – N_2H_4CS".

Detailed description and analysis of the evolution of morphology of lead sulfide films chemically deposited from the reaction bath with varied content of NH_4I was considered in our previous work [41]. It was shown, that adding ammonium iodide during CBD results in changes the shape of the grains (destruction of crystallite faceting), decrease in their size to about 400 nm and less, and increase in the fraction of nanoparticles up to 17%. In addition, it has been shown that ammonium iodide has proven itself as an effective dopant, providing high voltage sensitivity to IR radiation due to the inversion of conduction bands ($n \rightarrow p$) [41].

For study effect of $LaCl_3$ and NH_4I co-doping on properties of lead sulfide films fixed concentration of lanthanum chloride of 1 mM and varied content of ammonium iodide from 0.05 to 0.25 M were added into the reaction solution. The choice of lanthanum salt concentration is determined by the fact that in this case the formation of a more homogeneous film with the maximum number of nanocrystallites is ensured (Figs 5a, b). The morphology evolution of the synthesized PbS(La, I) films deposited in the presence of a combined additive of lanthanum chloride and ammonium iodide is shown in Fig. 6.

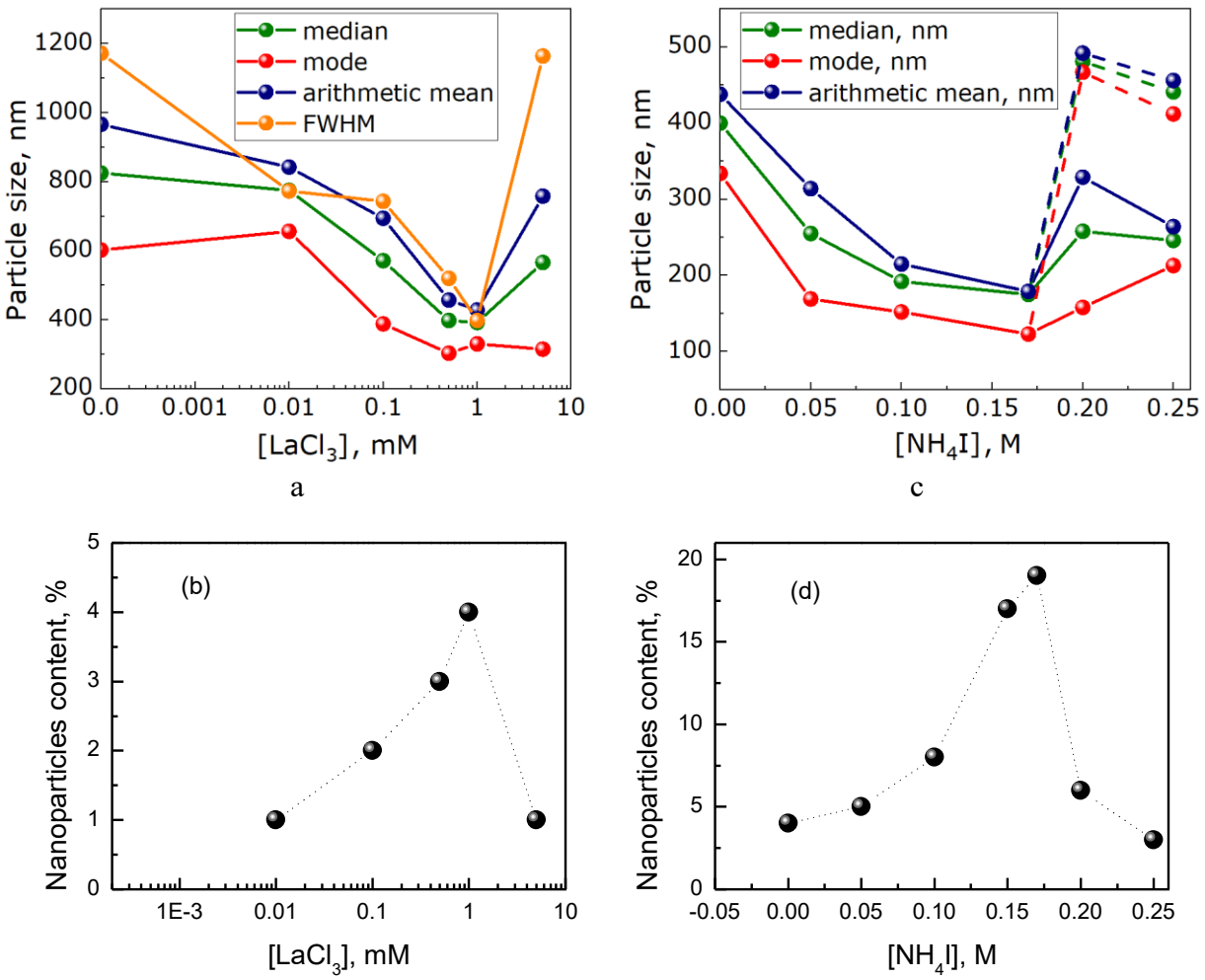


Fig 5 Quantitative values of statistical characteristics of the lognormal distribution of grain sizes (a, c) and content of nanoparticles (b, d) in PbS(La) (a, b) PbS(La,I) (c, d) films on the concentration of $LaCl_3$ (a, b) and NH_4I at fixed 1 mM $LaCl_3$ (c, d), respectively. In panels (a, c) median, mode, arithmetic mean parameter μ, and FWHM are shown.

The adding of 0.05 and 0.10 M NH_4I into the reaction bath leads to the formation of misoriented crystallites with flower-shaped crystallites, a significant decrease in the grain size, and a narrowing of the particle size distribution (Figs. 6 b, c). Under these conditions, crystallites with a size of 100-400 nm predominate and their proportion reaches near 80 and 65%, respectively. At that on the tops of many grains, light stepped growths and small embryonic blocks are formed (Fig. 6c). It indicates a strong effect of iodide ions on the nucleation and growth processes.

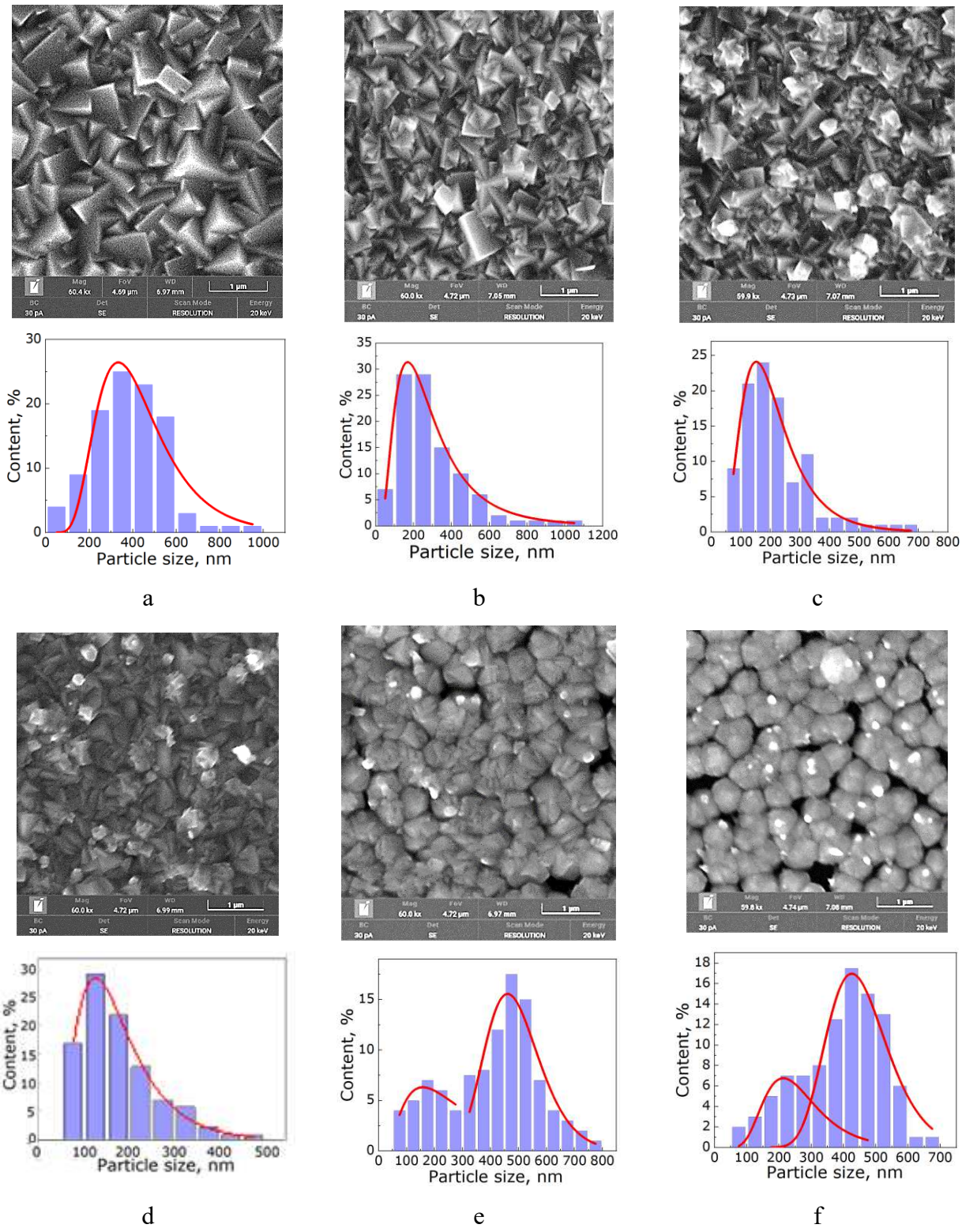


Fig. 6 SEM images and histograms of crystallite size distribution in PbS(La, I) films deposited from reaction bath contained 1 mM $LaCl_3$ and varied concentration of NH_4I: 0 (a), 0.05 (b), 0.10 (c), 0.17 (d), 0.20 M (e), and 0.25 M (f)

The PbS(La, I) film formed in the presence of a combined additive 1 mM $LaCl_3$ with 0.17 M NH_4I is characterized by a mosaic microstructure containing conglomerates of several (two, three, or more) submicron grains (Fig. 6d). The stepped film relief observed in the SEM images is interpreted

by us as a consequence of intense secondary (surface) nucleation and subsequent grain growth from randomly located crystallization centers. Increasing the NH_4I concentration to 0.20 M in the reaction mixture leads to the formation of large conglomerates, between which uncovered substrate surfaces are observed (Fig. 6e). The observed clear bimodal size distribution, the presence of both large and small/dispersed particles, indicates the formation of two fractions and is regarded as an indicator of film instability, a harbinger of its degradation. For the PbS(La,I) film deposited from a reaction mixture containing 0.25 M NH_4I significant degradation of the morphology is observed (Fig. 6f): it is seen a loss of faceting of the crystallites and an appearance areas where substrate is not covered by the film. Formation of lead sulfide film from the reaction bath with an increased the ammonium iodide concentration to 0.30 M becomes impossible.

Analysis of the morphological characteristics of PbS(La, I) films (Fig. 6 and 5c,d) shows that the film deposited at presence of 0.17 M ammonium iodide has smallest size of particles: about 60 % of grains are of 100-250 nm in size and about 17 % particles are of nanoscale. Increasing the content of NH_4I to 0.20 and 0.25 M decreases the portion of nanoparticles to 4 and 2%, respectively; and the main size of grains rises to 300-550 nm indicating stabilization of the formation process. The dependence of the content of film-forming nanoparticles on the concentration of ammonium iodide at fixed 1 mM $LaCl_3$ has an extreme character (Fig.5d) with a maximum at [NH_4I]=0.17 mM. A similar situation was previously observed in PbS(I) films deposited from a reaction mixture with the addition of only ammonium iodide [42]: the film deposited at presence of 0.15 M NH_4I had the highest number of nanoparticles. It is worth noting that donor-acceptor doping with lanthanum and iodine ions provides an increase in the maximum number of nanoparticles by about 4 times compared to the introduction of lanthanum alone (Fig. 5).

Table 1 shows the content of the main chemical elements (Pb, S, I) in considered film determined by EDA. The undoped PbS film is characterized by an excess of lead (52.2 at.%) and a deficiency of sulfur (47.8 at. %). Adding lanthanum chloride into the reaction mixture has an insignificant effect on the composition of PbS film, maintaining an excess of lead compared to sulfur: for example in PbS(La) film deposited in the presence of 1 mM $LaCl_3$, the content of lead (51.8 at.%) and sulfur (48.2 at.%) ions is close to the corresponding values in the undoped film. At that lanthanum ions was not detected by EDX analysis (at least within the limits of determination error).

Adding NH_4I into the reaction bath results in appearance of iodine ions in PbS(I) films, content of which is about 2.7 at.% in the film deposited at presence of 0.15 M NH_4I. In PbS(La, I) films deposited from reaction mixtures with a fixed concentration of lanthanum salt (1 mM) and varying concentration of ammonium iodide from 0.05 to 0.20 M, iodine content increases monotonically up to 3.2 at.% at [NH_4I]=0.20 M. It is worth noting, that content of lead and sulfur

in PbS(La, I) films changes nonlinearly with increase of [NH_4I] (Table 1). Analysis of the of EDX data shows that there is a slight excess of metal (Pb) compared to chalcogen (S) in all the films, regardless of the type and amount of dopant introduced into the reaction mixture. At that the non-stoichiometry decreases and the ratio of sulfur and lead changes from Pb:S = 1.09 for the undoped PbS film to 1.05 for PbS(La,I) film deposited in the presence of 0.17 M NH_4I.

Table 1 Elemental content in PbS, PbS(La), PbS(I) and PbS(La, I) films deposited from an ammonia-citrate reaction mixture at 353 K for 90 minutes and conductivity type

Film	[NH_4I], M	[$LaCl_3$], mM	Elemental content, at.%			Conductivity type
			Pb±0.5	S±0.4	I±0.3	
PbS	-	-	52.2	47.8	-	*n*
PbS(La)	-	1	51.8	48.2	-	*n*
PbS(I)	0.15	-	50.1	47.2	2.7	*p*
PbS(La, I)	0.05	1	50.9	47.7	1.4	*p*
PbS(La, I)	0.10	1	50.4	47.4	2.2	*p*
PbS(La, I)	0.15	1	50.1	47.1	2.8	*p*
PbS(La, I)	0.17	1	49.7	47.3	3.0	*p*
PbS(La, I)	0.20	1	49.8	47.0	3.2	*p*

Since oxygen is part of the composition of glass substrates used in present work, it is impossible to determine the presence of oxygen in the film by EDA. However surface sensitive FTIR spectra let determine oxygen-containing phase as it will be shown below.

3.4. Photoelectric properties

The nonequilibrium nature of CBD process of lead sulfide films, which involves a colloidal stage causing size effects and appearance of dynamic (lattice distortions) and static (vacancies, dislocations, crystal boundaries, microcracks, pores) defects, is enhanced at presence of a combined donor-acceptor additive (lanthanum ions La^{3+} and iodide ions I^-). These additives not only influence the thickness, morphology (size and shape of grains), the content of nanoscale particles, and the elemental composition of PbS(La), PbS(I), and PbS(La, I) films, but also affect the electrical properties of the layers. To assess this influence, the functional properties of the films were measured which are dark resistance R_d and photosensitivity to IR radiation, i.e. voltage sensitivity U_s.

Before analyzing the photovoltaic characteristics, let's consider how the addition of a dopant into the reaction mixture affects the conductivity type of the deposited films. Adding

$LaCl_3$ into the reactor does not affect the type of charge carriers, but the addition of NH_4I causes a change from *n*-type of conductivity to *p*-type for all considered films with any content of iodine (Table 1). The obtained results are consistent with the results presented in [32, 33, 37, 39, 41]. The change from the *n*-type conductivity of PbS and PbS(La) films to the *p*-type one in PbS(I) and PbS(La, I) films can be explained by the phenomenon of carrier self-compensation [73] caused by an energetic advantage of the formation of intrinsic lattice defects (vacancies, interstitial atoms, vacancy-impurity complexes) upon the introduction of halogens with a deep donor effect during CBD, as it was shown in particular for bromine [6] or iodine [74].

Figure 7 shows the dependences of the dark resistance R_d and the voltage sensitivity U_s of 5×5 mm elements based on PbS(La) (panels (a) and (c)) or PbS(I) and PbS(La, I) films (panels (b) and (d)) on the concentration of additives in the reaction bath. As can be seen from Fig. 7a, the value of R_d of PbS(La), PbS(I), and PbS(La,I) films has an extreme character. For PbS(La) films, the maximum dark resistance is achieved at 1 mM $LaCl_3$. In the case of varying the ammonium iodide content in the reaction bath (PbS(I) and PbS(La,I) films), the highest R_d value is observed at $[NH_4I]$ = 0.15-0.17 M. At that, dark resistance of PbS(La,I) films is significantly higher compared to that of PbS(I) and PbS(La) films over the entire studied range of NH_4I concentration. The maximum R_d value of PbS(La,I) films is approximately 1.5 times higher than that of PbS(La) films and almost 3 times higher than that of PbS(La,I) films. The highest value of R_d of PbS(La,I) films can be associated with the maximum content of nanoscale particles (Fig. 5) and is consistent with electron microscopy data indicating morphological heterogeneity of the films (Fig. 6d).

A similar extreme character is also seen in the dependence of the voltage sensitivity U_s on the NH_4I concentration for PbS(I) and PbS(La, I) films with a maximum at $[NH_4I]$=0.17 M (Fig. 7b), while for PbS(La) films a monotonic increase of U_s from 20 to 200 μV is observed with an increase in $LaCl_3$concentration from 0 to 10 mM. The maximum value of U_s for PbS(I) films is about 2000 μV, for PbS(La, I) it reaches U_s = 5600 μV being by 2.8 times highest than that PbS(I) films. The increase in the voltage sensitivity of PbS(La,I) films can be attributed to the formation of an optimal ratio between the bulk conductivity of grains and the barrier properties of intergranular boundaries, as well as the contribution from the grain surface. As shown in our previous studies [39, 75], photoactive phases (I_2O_5, I_2O_4, IO_3^-) forming on the grain surface of the studied films play a major role in explaining the high voltage sensitivity.

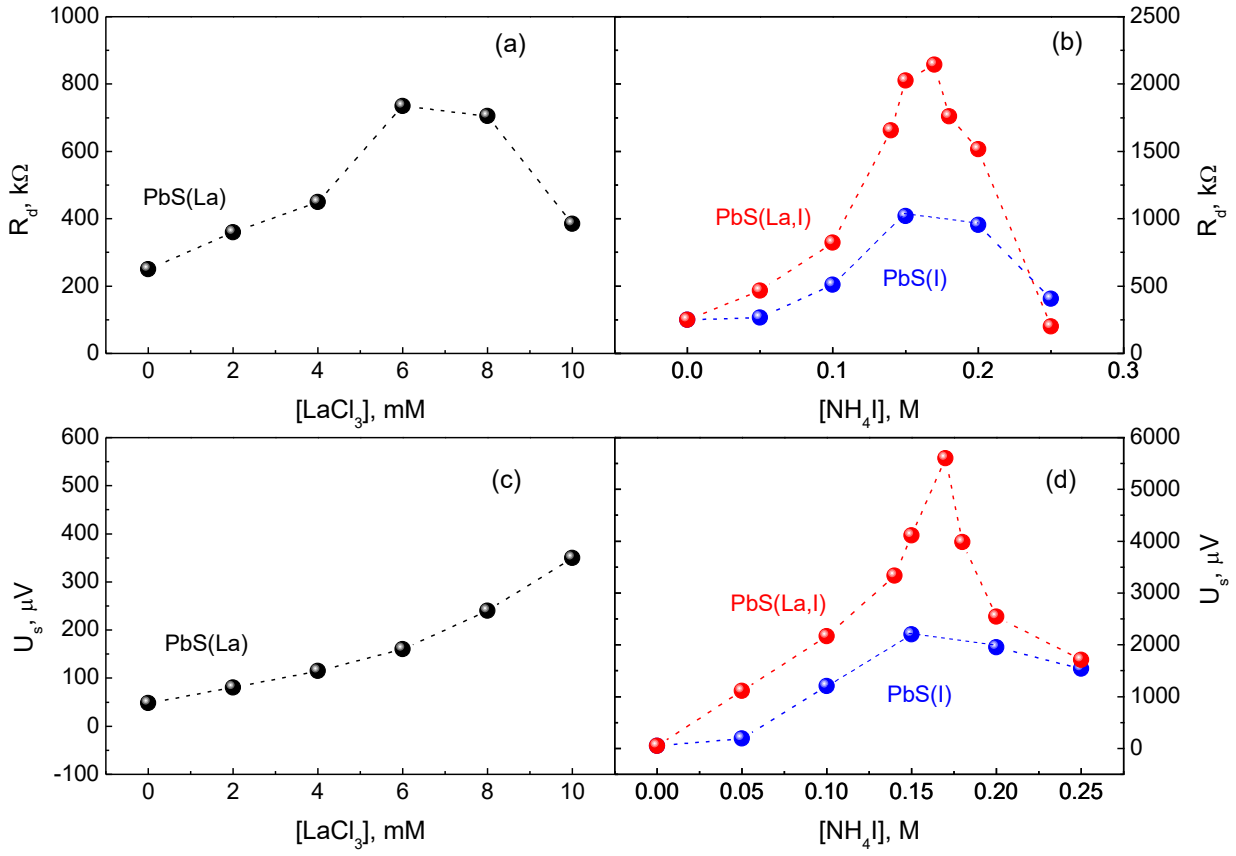


Fig. 7 Dependence of the dark resistance R_d (a, b) and voltage sensitivity U_s (c, d) of PbS(La) films on the concentration of $LaCl_3$ (a, c) and PbS(I) and PbS(La, I) films on the concentration of ammonium iodide in the reaction mixture at 1 mM $LaCl_3$ (b, d)

3.5. FTIR spectroscopy

FTIR spectroscopy was used to detect impurity chemical compounds on the surface of PbS, PbS(I), and PbS(La, I) films (Fig.8). For all discussed film the pronounced absorption lines are odserved at 732-760, 1938-1946 cm^{-1} indicating the presence of PbO oxide (718.4 cm^{-1} [76]) and $PbCN_2$ cyanamide (1950 cm^{-1} [77]). The formation of the PbO impurity phase can be explained by the oxidation of lead sulfide according to the reaction

$$PbS + 3/2O_2 = PbO + SO_2. \quad (10)$$

Lead cyanamide $PbCN_2$ is a consequence of the hydrolytic decomposition of thiourea in the reaction mixture with pH ≈ 11.8-12.2 according to reaction

$$N_2H_4CS = H_2S + H_2CN_2, \quad (11)$$

which results in the formation of CN_2^{2-} ions capable of interacting with Pb2+ ions in accordance with the reaction

$$H_2CN_2 + Pb^{2+} + 2OH^- = PbCN_2 + 2H_2O. \quad (12)$$

The absorption band at 942 cm^{-1} detected only in the undoped PbS film corresponds to the stretching vibrations of the sulfate ion SO_4^{2-} with a slight shift to the low-frequency region

compared to the frequency of 966 cm^{-1} [89], indicating the presence of lead sulfate $PbSO_4$ formed during the oxidation of lead sulfide

$$PbS + 2O_2 = PbSO_4. \quad (13)$$

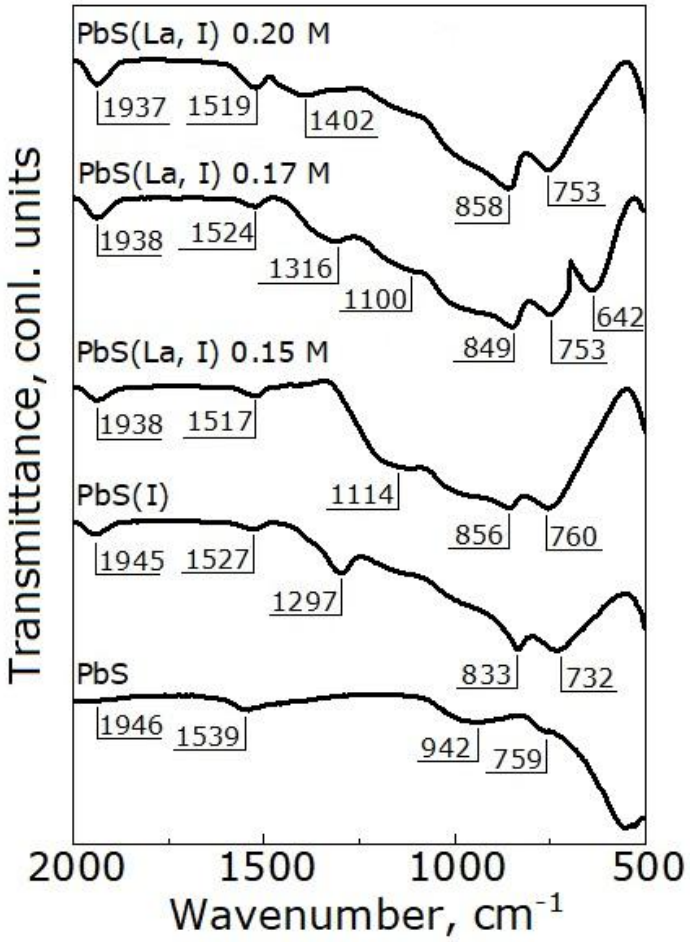


Fig. 8 FTIR spectra of undoped PbS film, PbS(I) film deposited at presence of 0.15 M NH_4I, and PbS(La,I) films deposited from the reaction bath contained 1 mM $LaCl_3$ and NH_4I of different concentration

In the spectra of PbS(I) and PbS(La, I) films, there is an absorption band in the frequency range of 835–858 cm^{-1}, which corresponds to diiodine pentoxide I_2O_5 [79]. This photoactive phase is a result of the appearance of PbO, which in an alkaline medium acts as an oxidizer of iodide ions I^- according to the reaction

$$4Pb^{2+}O + 2I^- + 2OH^- = 4Pb^0 + I_2O_5 + H_2O. \quad (14)$$

Increase in the concentration of ammonium iodide in the reactor to 0.20 M leads to a high-frequency shift of the absorption band from 833 cm^{-1} to 858 cm^{-1} and to the increase in its intensity. It can be interpreted as an increase in the content of I_2O_5 on the surface of PbS(La, I) film.

The band at 642 cm^{-1} is of special attention. This band is detected only on the surface of a PbS(La, I) film deposited from a reaction mixture containing 1 mM lanthanum chloride and 0.17 M ammonium iodide and most likely corresponds to the stretching vibrations of the La–O bond. In the works [80, 81] it was reported that absorption of La-O stretching appears at wave number 643 cm^{-1}, and La-O bending appears at 414-423 cm^{-1}. The same results was obtained in [82], where in the FTIR spectra of La_2O_3 gel the La-O bending and stretching vibrations was found at around 530–620 cm^{-1} and 950–1100 cm^{-1}, respectively. The FTIR spectra of nanoparticles La_2O_3 also showed bending and stretching modes at about 530-620 cm^{-1} and 950-1100 cm^{-1} [83]. In La/Si binary oxides gel system a characteristic decrease in the intensities of the absorbance bands at about 643 and 865 cm^{-1} (La–O stretching vibration) with decreasing quantity of lanthanum oxide was observed [84].

Due to the limited spectral range of our FTIR spectra (up to 500 cm^{-1}), we can only confirm the presence of the La–O stretching mode, which indicates the existence of a lanthanum oxide phase La_2O_3 on the surface of studied PbS(La, I) film. Evidence of the preferential formation of the lanthanum oxide form in the form of hydroxide $La(OH)_3$ compared to its sulfide during CBD is provided by its solubility product, equal to $SP = 2\times10^{-19}$, which is significantly lower than the solubility product of lanthanum sulfide La_2S_3 ($SP = 2\times10^{-13}$). In addition, there is a possibility of hydrolysis of lanthanum chloride $LaCl_3$ in an alkaline medium (pH = 12.2) according to the reaction

$$LaCl_3 + 3NH_4OH = La(OH)_3 + 3NH_4Cl \qquad (15)$$

with further hydrolysis leading to the release of lanthanum oxide

$$2La(OH)_3 = La_2O_3 + 3H_2O. \qquad (16)$$

The formation of the La_2O_3 phase is typical for lanthanum compounds confirming the participation in the modification of the surface layer of PbS films, contributing to an increase in its gas sensitivity to hydrogen H_2.

In addition, the FTIR spectra of PbS(La, I) films deposited at presence of 0.17 and 0.20 M NH_4I have absorption bands with maxima at 1318 and 1402 cm^{-1} corresponding to the stretching vibrations of the C=S bond [85]. The IR spectra of all the films under study contain also absorption bands in the range of 1527–1538 cm^{-1} related to the vibrations of the acetate ions CH_3COO^- [86].

Lead or lanthanum compounds with iodine do not appear in the IR spectra of the samples studied. This is due to the low vibrational frequencies of the Pb-I and La-I bonds, which lie outside the operating range of the spectrometer used.

Thus, the obtained FTIR spectroscopy data indicate that an optically active phase I_2O_5 is formed on the surface of PbS(I) and PbS(La, I) films upon the introduction of either ammonium

iodide or a combined additive of ammonium iodide and lanthanum chloride into the reaction mixture. Simultaneous presence of two photoactive oxide phases I_2O_5 and La_2O_3 is detected only on the surface of PbS(La, I) film deposited from the reaction mixture containing 0.17 M NH_4I and 1 mM $LaCl_3$. This indicates a synergistic effect, i.e., a non-additive action of lanthanum chloride and ammonium iodide salts, leading to the formation, along with I_2O_5, of a new active center in the form of La_2O_3 on the surface of PbS(La, I) film, which provide the maximum voltage sensitivity of this film.

3.6. Structural data of PbS(La, I) films

To further understand the nature of the observed functional properties (in our case, the photoresponse) of the semiconductor and its suitability for creating optoelectronic devices, it is important to study the phase composition, crystal structure, and the resulting microdeformation. Therefore the XDR study of PbS, PbS(La), and PbS(La, I) films was carried out. Detailed study of the effect of adding NH_4I into the reaction bath on structural properties of PbS films was carried out in [41]. So we will not discuss structural data of PbS(I) films in detail in the present work, we will only briefly remind the main results: (i) the films have a cubic structure of the NaCl (*B*1) type; (ii) increase in the concentration of NH_4I in the reaction mixture to 0.4 M increases the lattice parameter from 0.59315(1) to 0.59442(3) nm, decreases the size of CSR from 249 to 65 nm, and increases microdeformation $<\Delta d/d>$ from 13.6×10^4 to 21.2×10^4; (iii) a texture of the PbS(I) films, i.e. the preferred crystallites orientation, corresponds to (200) plane.

The XRD patterns of PbS film and some of PbS(I), PbS(La), and PbS(La, I) films (Fig. 9) show a set of diffraction reflections characteristic of a face-centered cubic lattice of the NaCl type (*B*1, $Fm\bar{3}m$ space group). No reflections of other compounds are observed indicating the presence of only the crystalline phase of lead sulfide. The isotropic background of the XRD patterns, a fairly small reflection width, and the absence of a diffuse halo suggest that the films under study are polycrystalline and single-phase. It is seen that the intensity ratio of the (111) and (200) reflections of PbS(La), PbS(La,I) films differs from that of the undoped PbS film. For the PbS film, the reflections (111), (200) and (220) have the greatest intensity. It indicates presence of a predominant orientation of the film crystallites with these crystallographic planes lying along the substrate; the content of such crystallites is almost the same. It is in agreement with SEM image (Fig.4a) in which vertices, edges and faces of cubic crystallites are visible in approximately equal numbers.

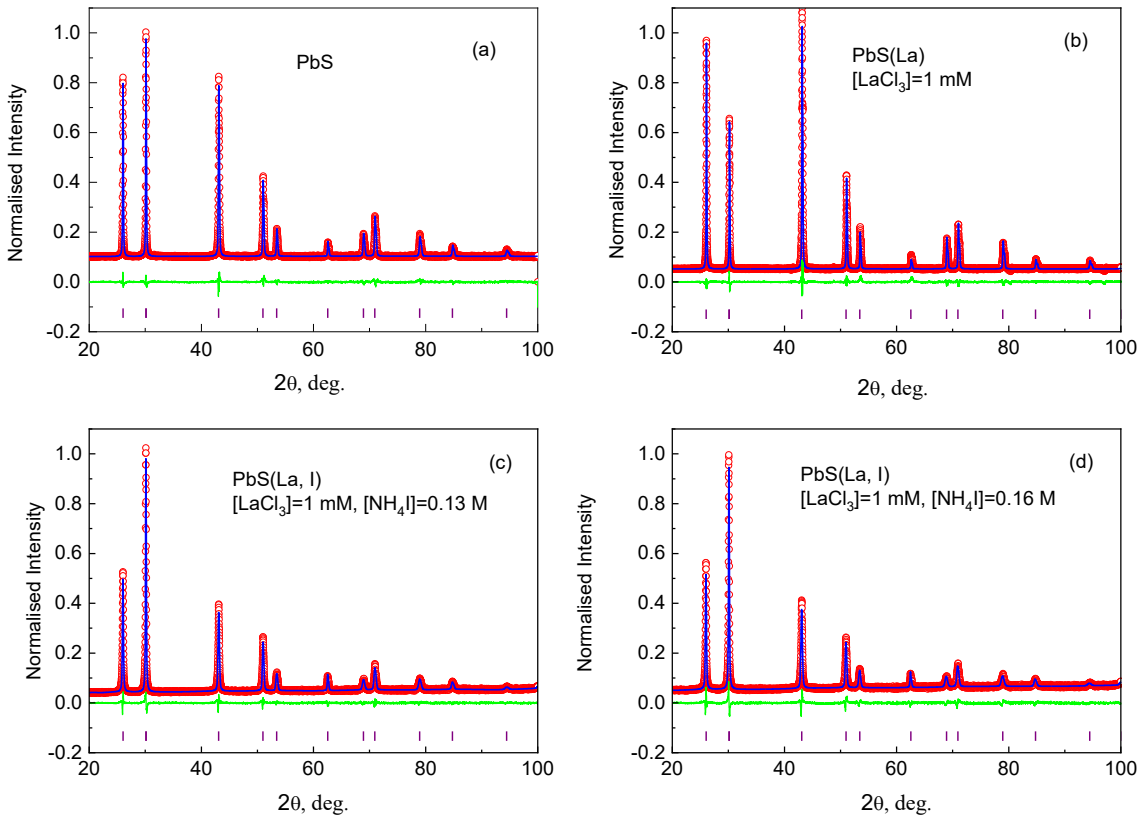


Fig. 9 XRD patterns of PbS (a), PbS(La) deposited from a reaction mixture containing 1 mM $LaCl_3$ (b), and PbS(La, I) films deposited from a mixture with 1 mM $LaCl_3$ and 0.13 M NH_4I (c) or 0.14 M NH_4I (d)

Adding $LaCl_3$ into the reaction bath results in change the intensity ratio of the reflections and reflection (111) and (220) become higher (Fig. 9b) and it is manifested in the SEM image (Fig. 4e) where vertices and edges of cubic crystallites of lead sulfide are seen predominantly. The PbS(La, I) films deposited at presence both $LaCl_3$ and NH_4I in the reaction bath are characterized more intensive (200) reflections (Figs. 9c, d) and are mainly formed from crystallites with the (200) orientation. The degree of texture of the films, i.e., the relative proportion of crystallites with a preferred orientation, is given in Tables 2. Despite the partial destruction of the crystallite faceting in PbS(La,I) films, which is visible in the SEM images (Fig. 6), the degree of texture in these films is higher and remains almost unchanged with varying NH_4I content in the reaction bath.

A comprehensive analysis of the experimental XRD patterns was carried out, taking into account the individual features of the structural state of the lead sulfide films, broadening of reflections, film thickness, and the preferred orientation of grains; corrections for the shift in the zero of the spectrum, deviation from the scattering plane, angular dependence, etc. were considered also. As a result, good agreement of the profiles of the experimental and calculated

XRD patterns of all the synthesized films was obtained. The structural parameters of the PbS(La) and PbS(La, I) films, microdeformations, size of CSR, Debye-Waller factor obtained from fitting are presented in Tables 2.

Table 2 Crystal lattice parameter a_{B1}, factor of preferential orientation along the main crystallographic directions P_{hkl}, average value of microdeformations $<\Delta d/d>$, size of coherent scattering regions (CSR) D and Debye factor U_{iso} of PbS, PbS(I), PbS(La), and PbS(La, I) films deposited from a reaction mixture containing $LaCl_3$ and different concentration of NH_4I

Film	$[LaCl_3]$, mM	$[NH_4I]$, M	P_{hkl}, %			a_{B1}, nm	$<\Delta d/d>$ $\times10^{-3}$	D, nm	$U_{iso}\times10^{-2}$	
			111	200	220				Pb	S
PbS	-	-	0.733	0.841	1.249	0.59365(1)	3.6	249	1.65	2.08
PbS(I)	-	0.15	0.932	1.127	0.959	0.59388(1)	5.7	125	2.96	2.60
PbS(La)	0.01	-	1.086	0.423	1.231	5.93694(5)	3.9	198	3.25	2.57
	0.1		0.876	0.474	1.300	5.93792(4)	3.1	224	3.43	3.09
	0.5		0.764	0.417	1.415	5.93798(4)	3.1	223	3.04	2.55
	1.0		0.747	0.469	1.380	5.93863(4)	3.1	224	3.00	2.61
	5.0		0.932	0.523	1.268	5.93832(4)	3.2	237	3.24	2.70
PbS(La,I)	1.0	0.13	0.798	1.255	0.966	0.59387(1)	7.0	116	2.60	2.41
		0.14	0.843	1.247	1.011	0.59390(1)	7.2	105.2	2.51	2.41
		0.15	0.833	1.259	0.994	0.59394(1)	7.4	108.1	2.51	2.21
		0.16	0.851	1.258	1.013	0.59412(2)	7.6	97	2.62	2.11
		0.20	0.851	1.258	1.013	0.59428(2)	8.9	90	2.61	2.31

Let us consider the change in the lattice parameter of lead sulfide with increasing $LaCl_3$ salt content in the reaction bath for chemical deposition of PbS(La) films. Since the radius of La^{3+} ion is smaller than that of Pb^{2+} ion (r_{La3+}=1.06 Å and r_{Pb2+}= 1.19 Å), the crystal lattice should contract during isomorphic substitution. Besides this, vacancies appearing in the lead sublattice to compensate for the excess lanthanum charge also should result in the lattice contraction. However a slight increase in the parameter *a* is found (Fig. 10a), which let conclude that some of the lanthanum ions do not occupy the regular sites of the PbS matrix and are introduced into the octahedral or tetrahedral interstitials of the cubic lattice of lead sulfide. These interstitial ions cause a strong local expansion of the lattice. Reaching a plateau at $[LaCl_3]$ = 1

mM indicates the limit of lanthanum solubility in interstitials; excess reagent is located at grain boundaries or on the film surface.

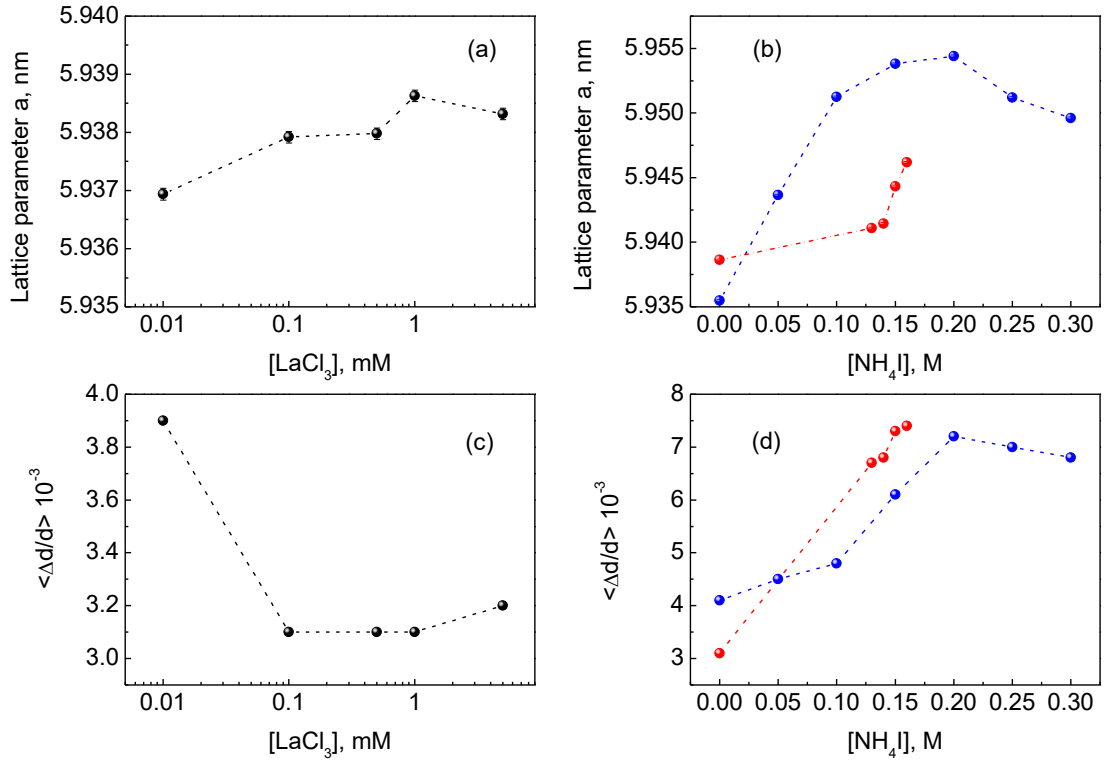


Fig. 10 Dependence of the lattice parameters and microdeformations in PbS(La), PbS(I) and PbS(La,I) films on the concentration of $LaCl_3$ (a, c), PbS(I) and PbS(La, I) films on the concentration of ammonium iodide in the reaction mixture at 1 mM $LaCl_3$ (b, d)

For the PbS(I) films the lattice parameter *a* nonmonotonically changes with increase in concentration of NH_4I in the bath, a maximum is observed at [NH_4I]=0.20 M (Fig.10b), which is probably associated with reaching the solubility limit and the transition of excess iodine into the interstices or the release of a second phase [41]. In the PbS(La,I) films increase in the value of *a* also increase with the concentration of NH_4I to 0.2 M at fixed content [$LaCl_3$]=1 mM. This is probably due to the partial substitution of sulfur ions (0.178 nm) by larger iodine ions (0.220 nm). It is worth noting that, according to theoretical calculations, approximately 1% of sulfur must be replaced to increase the lattice parameter to 0.5940 nm. Thus, only a portion of the iodine ions participates in the substitution, while the rest are localized on the grain or film surface in the form of iodine pentoxide, as shown by the FTIR spectra of PbS(I) and PbS(La, I) films. The Debye factor U_{iso} being the sum of the deviation of atoms from their stable position in the crystal lattice due to the influence of temperature, static disordered displacements and the occurrence of defects in the sublattices of lead and sulfur is almost unchanged with increase in NH_4I concentration (Table 2) and therefore indicates small rate of the substituted ions.

All processes occurring during PbS doping are also reflected in the internal state of the crystal lattice. In the PbS(La) films microdeformations of the lattice are caused by the introduction of lanthanum atoms into interstices (Fig. 10c). In the PbS(I) films, iodine ions replace sulfur atoms, which results in some displacements of ions from an equilibrium position in undoped PbS; these displacements increase, passing through a maximum at 0.2 M. Co-doping with $LaCl_3$ and NH_4I makes microdeformations greater due to the both mentioned processes. The rate of increase in $<\Delta d/d>$ in the PbS(La,I) films is close to that in the PbS(I) films (the slope is the same). These dependences (Fig. 10d) correlate well with changes in the lattice parameter (Fig. 10b).

Another parameter characterizing the specifics of polycrystalline film formation during CBD process is the CSR size, which characterizes the average size of crystalline block. As one can see from Table 2, the addition of $LaCl_3$, NH_4I or their combination into the reaction bath leads to different effects on the crystallite growth kinetics. Lanthanum chloride $LaCl_3$ causes a sharp increase in CSR, i.e. lanthanum initially stimulates block coarsening. Ammonium iodide NH_4I results in a monotonic and strong decrease in CSR. Iodine acts as a strong inhibitor of grain growth, fragmenting the crystalline structure. Co-doping with $LaCl_3$ and NH_4I produces decreases in CSR in the PbS(La, I) films with increasing iodine content in the mixture (Table 2). This trend is consistent with the SEM data for all films (Figs. 4 and 6), except for PbS(La, I) deposited from the reaction mixtures contained highest content of NH_4I (0.2 and 0.25 M). However, the values of the crystallite sizes from SEM and *D* differ. This is due to the fact that the CSR is a microscopic region of an ordered structure (a crystallite, a block, or a long-range order region) in a solid (crystal), within which X-ray scattering occurs coherently, creating constructive interference. Crystal lattice disorder typically exists at the crystallite boundaries, which results in the CSR size often being smaller than the actual crystallite size. In addition, crystallites can consist of several blocks, the size of which corresponds to the CSR.

3.7. Optical absorption spectra

To understand possible changes in the electronic structure and impurity levels of PbS(La,I) films that may be related to the photosensitive characteristics, the absorption spectra $\alpha(E)$ in the near-IR range near the absorption edge were studied. However, before considering the effect of the combined addition of $LaCl_3$ and NH_4I salts on the properties of the deposited lead sulfide films, it is necessary to understand the effect of each dopant individually. The effect of the introduction of ammonium iodide was previously studied in [41]. It was shown that the adding of NH_4I into the reaction bath leads to a sharp increase in the band gap E_g to approximately 0.8 eV, and a further increase in the NH_4I content does not affect the E_g value.

Figure 11 shows the $\alpha(E)$ absorption spectra of PbS(La) films deposited from reaction mixtures containing in addition 0.01-10 mM lanthanum chloride; the $\alpha(E)$ spectrum of an undoped PbS film is also shown for comparison. It is seen that the absorption edge remains almost unchanged. The E_g value was determined by the Tauc graphical method, in which the absorption spectra were plotted in the $(\alpha E)^2 - E$ coordinates applicable to semiconductors with direct interband transitions [87]; it is known that undoped PbS is a direct band gap semiconductor [88]. From the Tauc plot it is found that the band gap width changes slightly and is about 0.39-0.42 eV. Below the absorption edge at energies E<0.4 eV there is an impurity absorption band, which is observed even in undoped PbS near 0.3 eV and may be associated with sulfur vacancies [75] (Table 1) or with oxygen-containing phases [33], the existence of which is indicated by the FTIR spectroscopy. The position and the intensity of this band non-monotonically changes with the $LaCl_3$ content. Probably, different concentration of lanthanum chloride creates different conditions for the formation of solid phases of lead and lanthanum sulfides and hydroxides, including lanthanum oxide.

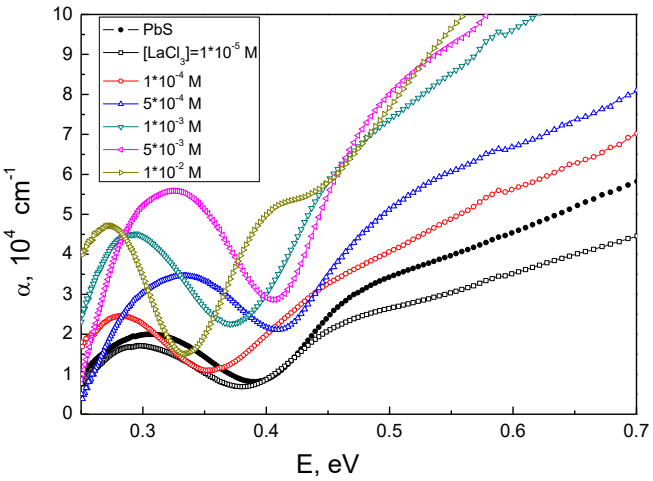


Fig 11 The absorption coefficient α spectra of PbS and PbS(La) films deposited for 90 minutes on glass substrates depending on the concentration of lanthanum chloride varied from $[LaCl_3]=10^{-5}$ to 10^{-2} M in the reaction mixture

Now let's consider the effect of the simultaneous introduction of iodine and lanthanum salts on the optical spectra (Figure 12a). For comparison, the absorption spectrum of PbS(La) film deposited at presence of 1 mM $LaCl_3$ is also shown. The introduction of NH_4I at a minimum concentration of 0.13 M, together with 1 mM $LaCl_3$, leads to a strong shift of the absorption edge to the high-energy region (by approximately 0.1 eV), and the appearance of an additional shoulder at 0.33 eV at the high-energy edge of the impurity band. With increasing NH_4I concentration, a noticeable shift of the absorption edge to higher energies occurs, and the additional absorption at the high-energy edge of the impurity band at 0.3-0.4 eV increases.

Subtraction of the spectrum of the film deposited from the bath with the lowest concentration of [NH_4I]=0.13 M from the $\alpha(E)$ spectra of the films deposited from solutions with different concentrations of NH_4I allows one to see an evolution of the optical spectra caused by iodine adding. This additional absorption has the form of a clearly defined band that increases in intensity, and its maximum shifts slightly toward higher energies to 0.42 eV for [NH_4I]=0.20 M (Figure 12b). Note that such an evolution of the absorption coefficient with varying ammonium iodide content differs from the case of adding only iodine salt to the reaction bath reported in [41] where any clearly defined band before the absorption edge was not observed. At the same time, for PbS films deposited in the presence of both NH_4I and $NiCl_2$, there was a similar band at 0.47 eV [39]; in the spectra of films deposited from a reaction bath with the simultaneous addition of NH_4I and $CrCl_3$ similar band was observed near 0.35 eV [89]. Taking into account the observed evolution of the absorption spectrum of PbS(La, I) films with NH_4I concentration and the fact that, according to the EDX data, lanthanum was not detected in these films (at least within the measurement accuracy), the discussed absorption band with a maximum at 0.36-0.42 eV should be attributes to iodine ions, which form an impurity level in the band gap.

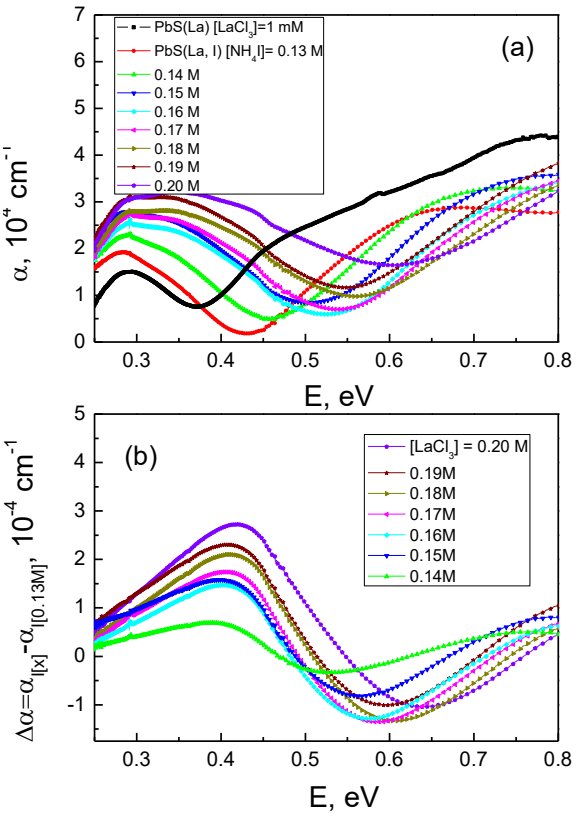


Fig. 12 Absorption coefficient α spectra of PbS(La, I) films deposited for 90 minutes on glass substrates depending on the concentration of ammonium iodide varied from [NH_4I]=0.13 to 0.2 M in the reaction mixture at a content of [$LaCl_3$]=1 mM (a) and the result of subtracting the $\alpha(E)$ spectrum of PbS(La, I) film with 0.13 from the spectra of films deposited with varied concentration of $LaCl_3$ (b)

Figure 13 shows the intensities of this additional band at 0.36-0.42 eV as a function of the NH_4I concentration in the reaction bath. The same Figure 13 also shows the dependence of the iodine content in the film, determined by EDX. It is seen that although all values monotonically increase with the content of NH_4I in the solution, the character of the dependencies slightly differs. This may be due to the mentioned above fact that not all iodine determined from the EDX data enters the crystal lattice of the formed lead sulfide, but part of it forms the I_2O_5 phase, which is responsible for the high photoresponse of PbS(La,I) films.

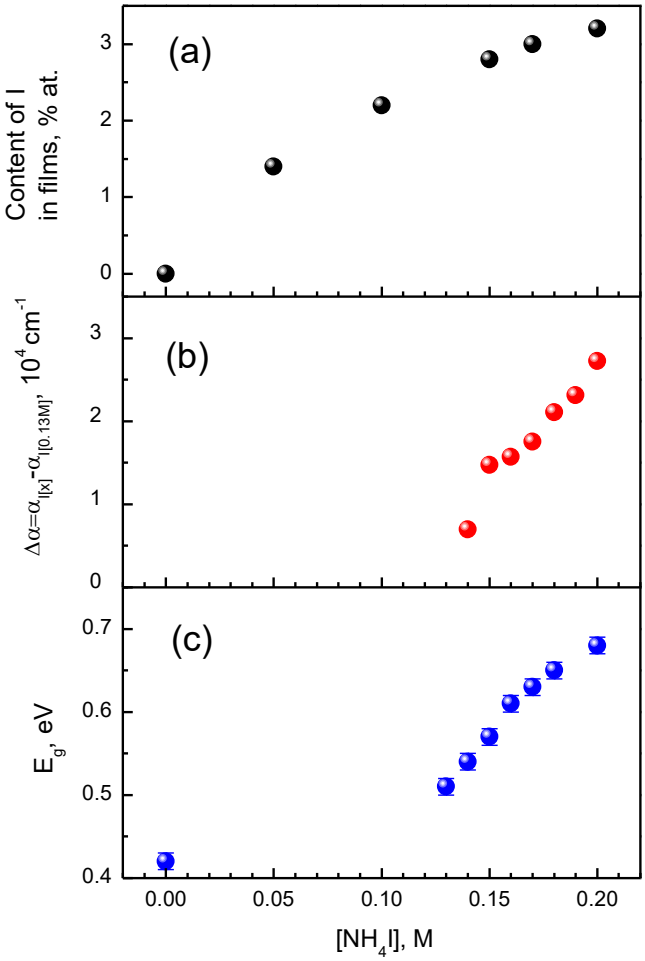


Fig. 13 Iodine content in PbS(La, I) films according to EDX data (a), the intensity of the additional absorption band with a maximum at 0.36–0.42 eV (b), and E_g value (c) depending on the concentration of NH_4I in the reaction bath additionally containing 1 mM $LaCl_3$

Let us now consider how varying the NH_4I concentration at a fixed 1 mM $LaCl_3$ affects the band gap. The E_g value was determined using the Tauc graphical method with extrapolation of the linear portions of the spectra to the energy axis (Figure 14). The E_g values estimated from the Tauc plot are presented in Table 3 and also are plotted in Figure 12d. It can be seen that, just like the lattice parameters and the intensity of the additional band, the band gap increases

monotonically with increasing NH_4I concentration in the reaction bath. Note that this tendency differs from the trend observed previously in the PbS(I) films deposited from similar reaction baths with varying NH_4I without the addition of other dopants reported in [41], in which the band gap remained almost unchanged in the NH_4I concentration range from 0.05 to 0.3 M. A comparison of the present results with the data of [41] allows us to conclude that the simultaneous adding the iodine and lanthanum salts leads to a significantly smoother and more continuous increase in the band gap. Such a change in E_g with the proposed doping of NH_4I and $LaCl_3$ can be used for controlled modification of the band gap of lead sulfide.

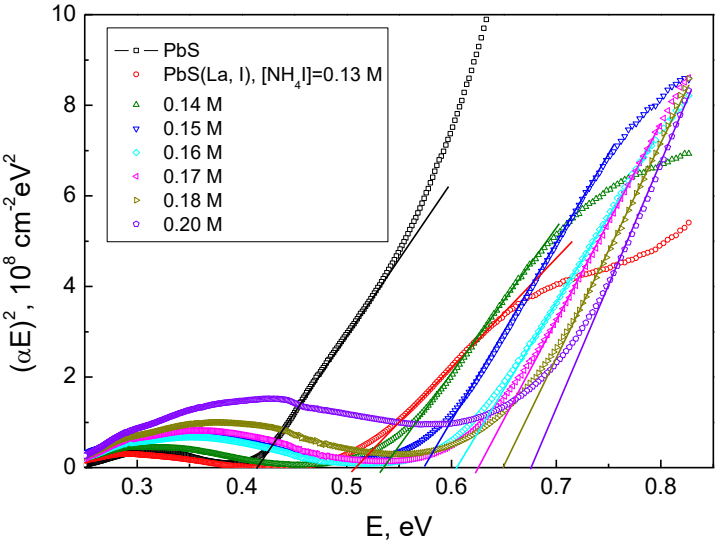


Fig. 14 Absorption spectra of PbS(La, I) films deposited at [$LaCl_3$]=1 mM and NH_4I with concentration varied from 0.13 to 0.2, plotted in coordinates $(\alpha E)^2$ vs E. Straight lines correspond to the extrapolation of the linear sections of the obtained curves to determine the E_g values

Table 3 Dependence of the band gap on the concentration of NH_4I at 1 mM $LaCl_3$

[NH_4I], M	0	0.13	0.14	0.15	0.16	0.17	0.18	0.20
E_g, eV	0.42	0.51	0.54	0.57	0.61	0.63	0.65	0.68

It is important to note, that the band gap of La_2O_3, PbO, and I_2O_5-contained phase, which were found by FTIR spectroscopy as impurity is significantly greater than that of determined for our PbS(La, I) films: E_g for La_2O_3 reported in literature is varied from 3.64 [90, 91] to 5.3 eV [92], E_g for lead oxide is about 2.2 eV (for α-PbO) and 2.9 eV (for β-PbO) [93, 94], and E_g for iodate materials (for example $Mg(IO_3)_2$ or $Zn(IO_3)_2$) is about 2.9 – 3.9 eV [95]. Consequently, the change in the band gap width of the PbS(La, I) films with the simultaneous adding of $LaCl_3$ and NH_4I is not associated with the appearance of mentioned impurity phases on the surface of the crystallites.

As noted above, the band gap E_g of the considered PbS(La, I) films increases monotonically with doping. At the same time, the voltage sensitivity U_s versus [NH_4I] exhibits an extreme behavior, with maximum values for films deposited in the presence of 0.17 M NH_4I. The dependence of the fraction of nanoparticles in the films on the iodine salt concentration, determined from SEM data, has a similar pattern (Fig. 5). It let conclude, that the main factor responsible for the enhanced photoresponse is achieving the optimal (maximal) fraction of nanoparticles in PbS(La, I) films as a result of the inhibitory effect of the simultaneous addition of NH_4I and $LaCl_3$.

Conclusions

PbS(La,I) films up to 180~280 nm thick were obtained on glass substrates by chemical bath deposition from reaction mixtures containing 1 mM $LaCl_3$ and 0.05-0.20 M NH_4I. The iodine content in these films increased from 1.4 to 3.2 at.%, while lanthanum was not detected by EDX analysis.

X-ray diffraction analysis showed that PbS(La, I) films contained only a crystalline phase with a face-centered cubic lattice similar to NaCl ($B1$, $Fm\bar{3}m$ space group). The increase in the crystal lattice parameter was due to the partial substitution of larger iodine ions for sulfur ions. Theoretical calculations show that no more than ~1% of sulfur is involved in substitution, while the remaining iodine ions are localized on the film surface as iodine pentoxide I_2O_5, the presence of which is confirmed by FTIR spectra.

The deposited PbS(La,I) films do not require additional photosensitization procedures and are characterized by high voltage sensitivity to IR radiation (up to 5600 μV) with R_d no more than 2150 kOm, due to the formation of a combination of lanthanum oxides La_2O_3 and iodine I_2O_5 on the surface.

Optical studies have shown that the introduction of lanthanum salt alone has no effect on the band gap, and that the E_g value increases with the simultaneous introduction of $LaCl_3$ and NH_4I into the reactor. However, the change in E_g is not the primary reason for the improved photosensitive properties of PbS(La, I) films. A comparison of the complex of obtained data indicates that the main factor influencing the achievement of a high photoresponse in the form of high voltage sensitivity is an increase in the proportion of nanoparticles in the composition of the formed polycrystalline films.

Funding

This work was carried out with the financial support of the Ministry of Science and Higher Education of the Russian Federation (theme № FEUZ-2026-0008).

CRediT authorship contribution statement

L.N. Maskaeva: Writing – review & editing, Writing – original draft, Supervision, Methodology, Conceptualization**, T.S. Bokov:** Investigation**, E.V. Mostovshchikova:** Writing – review & editing, Writing – original draft, Investigation, Formal analysis**, V.I. Voronin:** Writing – original draft, **O.S. Eltsov**: Writing – original draft, Investigation, Formal analysis, Formal analysis **A.V. Pozdin:** Investigation, Formal analysis**, I.N. Miroshnikova:** Supervision, Conceptualization**, I.D. Lobov:** Investigation, Formal analysis**, T. A. Kuznetsova:** Investigation.

Declaration of competing interest

The authors declare that they have no known competing financial interests or personal relationships that could have appeared to influence the work reported in this paper.

Data availability

Data will be made available on request.

References

1. R. Bai, D. Kumar, S. Chaudhary, D.K. Pandya, Highly crystalline p-PbS thin films with tunable optical and hole transport parameters by chemical bath deposition, Acta Mater. 131, 11–21 (2017) https://doi.org/10.1016/j.actamat.2017.03.062

2. R.B. Schoolar, J.R. Dixon, Optical constants of lead sulfide in the fundamental absorption edge region, Phys. Rev. 137, A667 (1965) https://doi.org/10.1103/PhysRev.137.A667

3. M. Kord, K. Hedayati, M. Farhadi, Green synthesis and characterization of flower-like PbS and metal-doped nanostructures via hydrothermal method, Main Group Met. Chem. 40, 35–40 (2017) https://doi.org/10.1515/mgmc-2016-0046

4. A.N. Fouda, M. Marzook, H.M. Abd El-Khalek, S. Ahmed, E.A. Eid, A.B. El Basaty, Structural and optical characterization of chemically deposited PbS thin films, Silicon. 9, 809–816 (2017) https://doi.org/10.1007/s12633-015-9399-z

5. J.B. Kwon, M. Han, D.G. Jung, S.H. Kong, D. Jung, High sensitivity shortwave infrared photodetector based on PbS QDs using P3HT, Nanomater. 11, 2683–2691 (2021) https://doi.org/10.3390/nano11102683

6. E.M. Larramendi, O. Calzadilla, A. Gonzalez-Arias, E. Hernandez, J. Ruiz-Garcia, Effect of surface structure on photosensitivity in chemically deposited PbS thin films, Thin Solid Films. 389, 301–306 (2001) https://doi.org/10.1016/S0040-6090(01)00815-X

7. C. Abarbanel, R. Shneck, Z. Dashevsky, S. Rotman, The development of infrared photosensitive material based on polycrystalline PbS films. MRS Proc. 607, 353 (1999) https://doi.org/10.1557/PROC-607-353

8. P.M. Khanzode, D.I. Halge, V.N. Narwade, J.W. Dadge, K.A. Bogle, Highly photoresponsive visible light photodetector using nano PbS thin film on paper, Optik. 226, 165933 (2021) https://doi.org/10.1016/j.ijleo.2020.165933

9. P.M. Khanzode, D.I. Halge, V.N. Narwade, K.D. More, S.U.R. Begum, S. Taha, S. Jejurikar, K.A. Bogle, Paper based photo-detector using nano-crystalline lead sulfide thin film, AIP Confer. Proc. 2269, 030104 (2020) https://doi.org/10.1063/5.0019617

10. K. Paulraj, S. Ramaswamy, N. Chidhambaram, H. Algarni, M. Shkir, S. AlFaify, Investigation of samarium-doped PbS thin films fabricated using nebulizer spray technique for photosensing applications, Superlattices Microstruct. 148, 106723 (2020) https://doi.org/10.1016/j.spmi.2020.106723

11. S.M. Ali, M.S. Al Garawi, S. Aldawood, S.A. Al Salman, S.S. Al Gamdi, Influence of gamma irradiation on the properties of PbS thin films, Radiat. Phys. Chem. 171, 108732 (2020) https://doi.org/10.1016/j.radphyschem.2020.108732

12. N.F. Shaafi, S.K. Muzakir, S.B. Aziz, M.F.Z. Kadir, S. Thanakodi, The effect of activated carbon additives on lead sulphide thin film for solar cell applications, J. Alloys Compd. 864, 158117 (2021) https://doi.org/10.1016/j.jallcom.2020.158117

13. M.S. Smagin, On some promising developments of night vision devices, sensible in NIR sub-band of infrared spectrum, Sens. Syst. 5, 43–47 (2016) (in Russian).

14. A.L. Urakov, E.L. Fischer, Temperature contrast of human body tissues improves their infrared visualization, Int. J. Appl. Fundam. Res. 6, 884–886 (2016) (in Russian)

15. V.F. Markov, L.N. Maskaeva, A.V. Schneider, R. Kh, R. Saryeva, Photodetectors based on halogen-containing lead sulfide films for flame detectors, J. Technosphere safety. 1, 32–37 (2015) (in Russian)

16. B. Jiang, X. Liu, Q. Wang, J. Cui, B. Jia, Y. Zhu, J. Feng, Y. Qiu, M. Gu, Z. Ge, J. He, Realizing high-efficiency power generation in low-cost PbS-based thermoelectric materials, Energy Environ. Sci. 13, 579–591 (2020) https://doi.org/10.1039/C9EE03410B

17. T. Fu, Research on gas-sensing properties of lead sulfide-based sensor for detection of NO_2 and NH_3 at room temperature, Sens. Act. B: Chem. 140, 116–121 (2009) https://doi.org/10.1016/j.snb.2009.03.075

18. T.V. Beatriceveena, E. Prabhu, A.S. Sree Rama Murthy, V. Jayaraman, K.I. Gnanasekar, Highly selective PbS thin film based ammonia sensor for inert ambient: In-situ Hall

and photoelectron studies, Appl. Surf. Sci. 456, 430–436 (2018) https://doi.org/10.1016/j.apsusc.2018.06.145

19. A. Hamdedein, A.A. Aboud, W.M.A. El Rouby, M.D. Khan, A.A. Farghali, M.H. Khedr, N. Revaprasadu, Effect of La doping on the structural and gas sensing properties of PbS thin films deposited by spray pyrolysis, IOP Conf. Ser. Mater. Sci. Eng. 1046, 012026 (2021) https://doi.org/10.1088/1757-899x/1046/1/012026

20. I.V. Zarubin, V.F. Markov, L.N. Maskaeva, N.V. Zarubina, M.V. Kuznetsov, Chemical sensors based on a hydrochemically deposited lead sulfide film for the determination of lead in aqueous solutions, J. Anal. Chem. 72, 327–332 (2017) https://doi.org/10.1134/S1061934817030145

21. E.K. Aktaev, Zh. Abdula, A. Kasym, A. Mustafayeva, A. Taishybekov, Remote control of atmospheric pollution by physical method, Intern. J. Appl. Fundam. Res. 5, 201–205 (2017) (in Russian).

22. V.I. Kaidanov, Resonance (Quasilocal) states in $A^{IV}B^{VI}$ semiconductors, Defect and Diffusion Forum. 103-105, 387–406 (1993) https://doi.org/10.4028/www.scientific.net/DDF.103-105.387

23. T.A. Alekseeva, V.F. Markov, L.N. Maskaeva, N.A. Tretyakova, The effect of cationic components of the reaction mixture on the kinetics, structure and properties of thin films of lead sulfide, Butlerov Commun. 17, 13–21 (2009) (in Russian)

24. M.C. Portillo, X. Mathew, H.J. Santiesteban, M.P. Castillo, O.P. Moreno, Growth and characterization of nanocrystalline PbS:Li thin films, Superlattices and Microstruct. 98, 242–252 (2016) https://doi.org/10.1016/j.spmi.2016.08.032

25. C. Rajashree, A.R. Balu, V.S. Nagarethinam, Enhancement in the physical properties of spray deposited nanostructured ternary PbMgS thin films towards optoelectronic applications, J. Mater. Sci. Mater. Electron. 27, 5070–5078 (2016) https://doi.org/10.1007/s10854-016-4396-6

26. A. Gassoumi, S. Alleg, N. Kamoun-Turki, Influencing the structural, microstructural and optical properties of PbS nanocrystalline thin films by Mg^{2+} doping, J. Mol. Struct. 1116 67–71 (2016) https://doi.org/10.1016/j.molstruc.2016.03.007

27. Y. Yücel, B. Beleli, The role of high Mg level as a dopant on the PbS nanostructures grown by the CBD method, Mater. Res. Express. 5, 056408 (2018) https://doi.org/10.1088/2053-1591/aac469

28. L.N. Maskaeva, E.V. Mostovshchikova, V.F. Markov, V.I. Voronin, Structural, optical, and photosensitive properties of PbS films deposited in the presence of $CaCl_2$, Semiconductors. 53, 165–171 (2019) https://doi.org/10.1134/S1063782619020179

29. E. Yücel, Y. Yücel, Effect of doping concentration on the structural, morphological and optical properties of Ca-doped PbS thin films grown by CBD, Optik. 142, 82–89 (2017) https://doi.org/10.1016/j.ijleo.2017.04.104

30. E. Yücel, Y. Yücel, Fabrication and characterization of Sr-doped PbS thin films grown by CBD. Ceram. Int. 43, 407–413 (2017) https://doi.org/10.1016/j.ceramint.2016.09.173

31. L.N. Maskaeva, P.S. Bogatova, V.F. Markov, A.D. Kutyavina, Yu.A. Babchenko, The effect of Sr^{2+} ions on precipitation kinetics, composition and morphology of PbS thin films, Butlerov Commun. 58, 141–148 (2019) (in Russian)

32. L.N. Maskaeva, E.V. Mostovshchikova, V.I. Voronin, E.E. Lekomtseva, P.S. Bogatova, V.F. Markov, Structure, optical, and photoelectric properties of lead-sulfide films doped with strontium and barium, Semiconductors. 54, 1230–1240 (2020) https://doi.org/10.1134/S1063782620100231

33. L.N. Maskaeva, E.V. Mostovshchikova, V.I. Voronin, A.V. Pozdin, I.O. Selyanin, I.A. Anokhina, V.F. Markov, Structural and electrical properties of PbS films doped with Cr^{3+} ions during chemical deposition, Semiconductors. 55, 855–864 (2021) https://doi.org/10.1134/S106378262110016X

34. N.A. Okereke, Study of the Optical, Electrical, Structural and Morphological Properties of Electrodeposited Lead Manganese Sulphide (PbMnS) Thin Film Semiconductors for Possible Device Applications, J. Mod. Mater. 8, 40–51 (2021) https://doi.org/10.21467/JMM.8.1.40-51

35. E.V. Mostovshchikova, V.I. Voronin, L.N. Maskaeva, I.V. Vaganova, N.A. Chufarova, V.P. Glazkov, Lead sulfide films with low iron doping: correlation between iron position and optical properties evolution, J. Alloy Compd. 852, 156932 (2021) https://doi.org/10.1016/j.jallcom.2020.156932

36. A. Ekinci, Ö. Şahin, S. Horoz, Chemical bath deposition of Co-doped PbS thin films for solar cell application, J. Mater. Sci. Mater. Electron. 31, 1210–1215 (2020) https://doi.org/10.1016/j.jallcom.2020.156932

37. L.N. Maskaeva, E.V. Mostovshchikova, V.F. Markov, V.I. Voronin, A.V. Pozdin, I.O. Selyanin, A.I. Mikhailova, Cobalt-Doped Chemically Deposited Lead-Sulfide Films, Semiconductors. 56, 91–100 (2022) https://doi.org/10.1134/S1063782622010122

38. M.A. Mora-Ramírez, M. Chávez Portillo, A. Reyes Díaz, O.P. Portillo Moreno, Synthesis, characterization and optical properties of Co^{2+} doped PbS nanocrystals, Optik. 238, 166629 (2021) https://doi.org/10.1016/j.ijleo.2021.166629

39. L.N. Maskaeva, A.V. Pozdin, E.V. Mostovshchikova, V.F. Markov, O.S. Eltsov, V.I. Voronin, I.V. Baklanova, P.N. Moshnikov, Low-temperature one-pot synthesis of nickel and

iodine-doped photosensitive thin films of lead (II) sulfide, J. Mater. Sci. Mater. Electron. 36, 1730 (2025) https://doi.org/10.1007/s10854-025-15816-6

40. C. Naşcu, V. Vomir, I. Pop, V. Ionescu, R. Grecu, The Study of Lead Sulphide Films. VI. Influence of Oxidants on the Chemically Deposited PbS Thin Films, Mater. Sci. Eng. B. 41, 235–240 (1996) https://doi.org/10.1016/S0921-5107(96)01611-X

41. V.F. Markov, L.N. Maskaeva, E.V. Mostovshchikova, V.I. Voronin, A.V. Pozdin, A.V. Beltseva, I.O. Selyanin, I.V. Baklanova, The influence of iodide addition on the composition, morphology, crystal structure, and semiconductor and photoelectric properties of PbS films, Phys. Chem. Chem. Phys. 24, 16085 (2022) https://doi.org/10.1039/D2CP01815B

42. V.A. Ulanov, R.R. Zainullin, T.A.H. Housheya, I.V. Yatsyk, Unusual Dependence of the Shape of Lines in the Electron Paramagnetic Resonance Spectra of Gd^{3+} Ions in a $Pb_{1-x}Gd_xS$ Semiconductor on Microwave Power: Shape Parameters and One Possible Nature of the Effect, Bull. Russ. Acad. Sci.: Phys. 85, 1337–1341 (2021) https://doi.org/10.3103/S1062873821120352

43. A.J. Kenyon, Recent developments in rare-earth doped materials for optoelectronics, Prog. Quant. Electron. 26, 225–284 (2002) https://doi.org/10.1016/ S0079-6727(02)00

44. A.R. Jha, Rare earth materials: properties and applications. CRC Press, N.W., 2014.

45. V.B. Baranovskaya, Y.A. Karpov, K.V. Petrova, N.A. Korotkova, Actual trends in the application of rare-earth metals and their compounds in the production of magnetic and luminescent materials: A review, Russ. J. Non-Ferr. Met. 62, 10–31 (2021) https://doi.org/10.3103/S1067821221010041

46. Y.A. Karpov, V.B. Baranovskaya, Problems of Analytical Control in the Production of Rare and Precious Metals, Russ. J. Non-Ferr. Met. 59, 374–384 (2018) https://doi.org/10.3103/S1067821218040089

47. I.N. Bazhukova, V.A. Pustovarov, A.V. Myshkina, M.V. Ulitko, Luminescent nanomaterials doped with rare earth ions and prospects for their biomedical applications (a review), Opt. Spectrosc. 128, 2050–2068 (2020) https://doi.org/10.1134/S0030400X20120875

48. H. Brunckova, L.A. Rocha, E.J. Nassar, S.B. Moscardini, H. Kolev, Luminescence properties of neodymium, samarium, and europium niobate and tantalate thin films, Luminescence. 37, 642 (2022) https://doi.org/10.1002/bio.4205

49. N.A. Korotkova, K.V. Petrova, V.B. Baranovskaya, M.S. Doronina, Analytical Control of Functional Materials Based on Rare-Earth Metals Using Mass Spectrometry Methods, J. Anal. Chem. 80, 785–793 (2025) https://doi.org/10.1134/S1061934825700200

50. M. Shkir, K.V. Chandekar, M.M. Hossain, B. Palanivel, N. Ahmed, I.M. Ashraf, H.H. Somaily, H. Algarni, S. Alfaify, Enhanced dielectric and electrical properties of PbS nanostructures facilely synthesized by low-cost chemical route: an effect of Ce doping

concentrations, Mater. Chem. Phys. 278, 125626 (2022) https://doi.org/10.1016/j.matchemphys.2021.125626

51. S. Ravishankar, A.R. Balu, V.S. Nagarethinam, Effect of Gd^{3+} Ions on the Thermal Behavior, Optical, Electrical and Magnetic Properties of PbS Thin Films, J. Electron. Mater. 47, 1271–1278 (2018) https://doi.org/10.1007/s11664-017-5910-1

52. K.V. Chandekar, F.H. Alkallas, A.B.G. Trabelsi, M. Shkir, J. Hakami, A. Khan, H E. Ali, N.S. Awwad, S. AlFaify, Improved linear and nonlinear optical properties of PbS thin films synthesized by spray pyrolysis technique for optoelectronics: An effect of Gd^{3+} doping concentrations, Physica B. 641, 414099 (2022) https://doi.org/10.1016/j.physb.2022.414099

53. K. Paulraj, S. Ramaswamy, S. Saravanakumar, M. Shkir, S. AlFaify, A. Khan, Comprehensive Study on Nebulizer-Spray-Pyrolyzed Eu-Doped PbS Thin Films for Optoelectronic Applications. J. Electron. Mater. 49, 5439–5448 (2020) https://doi.org/10.1007/s11664-020-08267-8

54. K. Paulraj, S. Ramaswamy, M. Shkir, I. S. Yahia, S. Mohamed, S. Hamdy, S. AlFaify, Analysis of neodymium rare earth element doping in PbS films for opto-electronics applications, J. Mater. Sci.: Mater. Electron. 31, 1817–1827 (2020) https://doi.org/10.1007/s10854-019-02698-8

55. R. Khan, M. Shkir, Improved opto-nonlinear and emission properties of spray pyrolysis grown Nd: PbS nanostructured thin films, Physica B. 627, 413612 (2022) https://doi.org/10.1016/j.physb.2021.413612

56. K. Paulraj, S. Ramaswamy, N. Chidhambaram, H. Algarni, M. Shkir, S. AlFaify, Investigation of samarium-doped PbS thin films for photosensing applications, Superlattices Microstruct. 148, 1067723 (2020) https://doi.org/10.1016/j.spmi.2020.106723

57. K. Paulraj, S. Ramaswamy, I.S. Yahia, A.M. Alshehri, H.H. Somaily, Hyun-Seok Kim, A. Kathalingam, Praseodymium doped PbS thin films for optoelectronic applications prepared by nebulizer spray pyrolysis, Appl. Phys. A. 126, 503 (2020) https://doi.org/10.1007/s00339-020-03686-0

58. K.V. Chandekar, M. Shkir, B. Palanivel, Z. Ahmad, H. Algarni, S. AlFaify, Comparative study of Pr-doped and undoped PbS nanostructures facilely synthesized for optoelectronic applications, Solid State Sci. 122, 106773 (2021) https://doi.org/10.1016/j.solidstatesciences.2021.106773

59. L.F. Koao, F.G. Hone, F.B. Dejene, Synthesis and characterization of PbS nanowires doped with Tb^{3+} Ions by using chemical bath deposition method, J. Nanostruct. Chem. 10, 1–7 (2019) https://doi.org/10.1007/s40097-019-00323-y

60. S. Chitra Devi, B. Sowmiya Devi, A.R. Balu, K. Devendran, M. Suganya, M. Sriramraj, Improved Haacke's quality factor, third order nonlinear susceptibility and specific capacitance realized for PbS thin films through La^{3+} doping, Ceram. Int. 49, 33793–33803 (2023) https://doi.org/10.1016/j.ceramint.2023.08.072

61. A.I. Okulova, L.N. Maskaeva, A.V. Pozdin, V.F. Markov, Thermodynamic study of the possibility of obtaining PbS – La_2S_3 films by hydrochemical deposition, Butlerov Commun. A. 77, 33–42 (2024) (in Russian)

62. H.M. Rietveld, A profile refinement method for nuclear and magnetic structures, J. Appl. Crystallogr. 2, 65–71 (1969). https://doi.org/10.1107/S0021889869006558.

63. B.H. Toby, R.B. Von Dreele, GSAS-II: the genesis of a modern open-source all purpose crystallography software package, J. Appl. Crystallogr. 46, 544–549 (2013) https://doi.org/10.1107/S0021889813003531

64. A.G. Khovansky, Chebyshev polynomials and their inversions, Mat. Pros. 17, 93–106 (2013) (in Russian)

65. G.K. Williamson, W.H. Hall. X-ray line broadening from filed aluminium and wolfram, Acta. Metall. 1, 22–31 (1953). https://doi.org/10.1016/0001-6160(53)90006-6.

66. V.F. Markov, L.N. Maskaeva, P.N. Ivanov, Hydrochemical deposition of metal sulfide films: modeling and experiment (Ural Branch of the Russian Academy of Sciences, Yekaterinburg, 2006), pp. 210 (in Russian)

67. V. F. Markov, L. N. Maskaeva, Calculating the boundary conditions of the formation of solid-phase metal sulfides and selenides by deposition with thio- and selenourea, Russian Journal of Physical Chemistry A. 86, 1288-1293 (2010) https://doi.org/10.1134/S0036024410080030

68. A.E. Martell, R.D. Hancock, Metal complexes in aqueous solutions (N.Y.-London: Plenum Press, 1996), pp.254 https://doi.org/10.1007/978-1-4899-1486-6

69. Yu.Yu. Lurie, Analytical Chemistry Handbook, (Khimiya, Moscow, 1989), pp. 448

70. J.N. Butler, Ionic equilibrium: solubility and pH calculations (John Wiley & Sons, New York, 1998), pp. 576

71. M. Jessica. Lange's Handbook of Chemistry enthalpy (London, 2017), pp. 1136

72. Yu.N. Kukushkin, Chemistry of coordination compounds (Vysshaya Shkola, Moscow, 1985) (in Russian).

73. V.I. Kaidanov, S.A. Nemov, Yu.I. Ravich, Self-compensation of electrically active impurities by intrinsic defects in IV-VI semiconductors, Semiconductors. 28, 223–237 (1994).

74. L.N. Maskaeva, A.V. Pozdin, A.Yu. Pavlova., Yu.V. Korkh, T.V. Kuznetsova, V.I. Voronin, K.E. Krivonosova, T.B. Charikova, V.F. Markov, Charge carrier transport in PbS films

doped with iodine, Phys. Chem. Chem. Phys. 26, 10641–10649 (2024) https://doi.org/10641-10649. :10.1039/D3CP06053E

75. L.N. Maskaeva, A.V. Beltseva, E.V. Mostovshchikova, V.I. Voronin, O.S. Eltsov, I.V. Baklanova, P.N. Mushnikov, K.S. Makaruk. V.F. Markov, Structural and functional features of photoactive lead sulfide films with iodine-containing impurity phases, Thin Solid Films. 817, 140654 (2025) https://doi.org/10.1016/j.tsf.2025.140654

76. K. Nakamoto, IR and RAMAN spectra of inorganic and coordination compounds, Mir, Moscow, 1991 (in Russian).

77. R.A. Nyquist, R.C. Kagel. Infrared Spectra of Inorganic Compounds (3800-45 cm^{-1}), Academic Press, New York, 1971.

78. G.L.J. Trettenhahn, G.E. Nauer, A. Neckel, Vibrational spectroscopy on the PbO-PbSO4 system and some related compounds: part 1. Fundamentals, infrared and Raman spectroscopy, Vib. Spectrosc. 5, 85–100 (1993) https://doi.org/10.1016/0924-2031(93)87058-2

79. O.H. Ellestad, T. Woldbek, A. Klekshus, P. Kleboe, E. Selte, Infrared and Raman Studies of Crystalline I_2O_5, $(IO)_2SO_4$, (IO)2SeO_4 and I_2O_4, Acta Chem. Scand. B. 35, 155–164 (1981) https://doi.org/10.3891/acta.chem.scand.35a-0155

80. H. Kabir, S.H. Nandyala, M.M. Rahman, M.A. Kabir, Z. Pikramenou, M. Laver, A. Stamboulis, Polyethylene glycol assisted facile sol-gel synthesis of lanthanum oxide nanoparticles: structural characterisation and photoluminescence studies, Ceram. Int. 45, 424-431 (2019) https://doi.org/10.1016/j.ceramint.2018.09.183

81. K. Li, Z. Liu, X. Shi, T. Wei, L.Q. Ma, J. Luo, Novel in Situ Method Based on Diffusive Gradients in Thin-Films with Lanthanum Oxide Nanoparticles for Measuring As, Sb, and V and in Water, J. Hazard. Mater. 383, 121196 (2020) https://doi.org/10.1016/j.jhazmat.2019.121196

82. H. Shafira, R.T. Yunarti, A. Saefumillah, Development Study of Binding Agent in Diffusive Gradient In Thin Films (DGT) Technique for Absorption of Phosphate Compounds using Nano-La_2O_3, Jurnal Kimia Valensi. 8, 280–288 (2022) https://doi.org/10.15408/jkv.v8i2.26952

83. S. Karthikeyan, M. Parthibavarman, Mustafa K.A. Mohammed, Safa H. Mohammed, M. Selvapandiyan, V.T. Srisuvetha, Morphology and Vibrational Modes of Lanthanum Oxide (La_2O_3) Nanoparticles Prepared with Reflux Routes at Different Reaction Times, Chem. Africa. 5, 1427–1432 (2022) https://doi.org/10.1007/s42250-022-00448-8

84. W. Nowicki, Z.S. Piskuła, P. Kuźma, P. Kirszensztejn, Synthesis and characterization of a binary system La_2O_3–SiO_2 prepared by combustion method, J. Sol-Gel Sci. Technol. 82, 574–580 (2017) https://doi.org/10.1007/s10971-017-4317-z

85. E. Pretsch, Spectra interpretation of organic compounds, John Wiley & Sons, 1997.

86. W.W. Scanlon, Recent advances in the optical and electronic properties of PbS, PbSe, PbTe and their alloys, J. Phys. Chem. Solids, 8, 423–428 (1959) https://doi.org/10.1016/0022-3697(59)90379-8

87. R. Saran, R.J. Curry, Lead sulphide nanocrystal photodetector technologies, Nat. Photonics. 10, 81–92 (2016) https://doi.org/10.1038/NPHOTON.2015.280

88. N.S. Kozhevnikova, L.N. Maskaeva, A.N. Enyashin, A.A. Uritskaya, A.V. Pozdin, V.I. Voronin, I.O. Selyanin, E.V. Mostovshchikova, V.F. Markov, The effect of sulfur precursor on the morphology, properties and formation mechanism of chemical bath deposited $Pb_{1+x}S$ thin solid films, Mater. Chem. Phys. 305, 127936 (2023) https://doi.org/10.1016/j.matchemphys.2023.127936

89. J. Tauc, R. Grigorovici, A. Vancu, Optical properties and electronic structure of amorphous germanium, Phys. Status Solidi B. 15, 627–637 (1966) https://doi.org/10.1002/pssb.19660150224

90. Nazia Erum, Muhammad Azhar Iqbal, Sadia Sagar, and Fareed un Nabi, Effect of Hydrostatic pressure on structural, electronic, optical and mechanical properties of Lanthanum Oxide (La_2O_3), Phys. Scr. 96, 115702 (2021) https://doi.org/10.1088/1402-4896/ac1474

91. Salman Ahmad , Amin Ur Rahman, Sikander Azam, Electronic structure modulation and enhanced optical-thermoelectric performance through relativistic band engineering in Eu-doped La_2O_3 (1.25 %, 2.25 %): Advancing PC-LED technology via GGA+U+SOC analysis, J. Phys. Chem. Solids. 201, 112621 (2025) https://doi.org/10.1016/j.jpcs.2025.112621

92. Yi Zhao; Koji Kita; Kentaro Kyuno; Akira Toriumi, Band gap enhancement and electrical properties of films doped with as high- gate insulators, Appl. Phys. Lett. 94, 042901 (2009) https://doi.org/10.1063/1.3075954

93. K. Hai, D. Tang, X.G. Wang, Effect of an oxidizing environment on the phase structure of lead oxide nanowires, AIP Adv., 3, 0221201–0221205 (2013) https://doi.org/10.1063/1.4793208

94. M. Baleva and V. Tuncheva, Laser-assisted deposition of PbO films, J. Mater. Sci. Lett. 13, 3 (1994). https://doi.org/10.1007/BF00680256

95. Akun Liang, Robin Turnbull, Placida Rodríguez-Hernandez, Alfonso Muñoz, M. Jasmin, Lan-Ting Shi, and Daniel Errandonea, General relationship between the band-gap energy and iodine-oxygen bond distance in metal iodates, Phys. Rev. Materials 6, 044603 (2022) https://doi.org/10.1103/PhysRevMaterials.6.044603